

Mirror energy difference in sd -shell nuclei using microscopic interactions

Chandan Sarma ¹, Praveen C. Srivastava ^{1,*}, Toshio Suzuki ^{2,3,4} and Noritaka Shimizu ⁵

¹*Department of Physics, Indian Institute of Technology Roorkee, Roorkee 247667, India*

²*Department of Physics, College of Humanities and Sciences,*

Nihon University, Sakurajosui 3, Setagaya-ku, Tokyo 156-8550, Japan

³*NAT Research Center, NAT Corporation, 3129-45 Hibara Muramatsu, Tokai-mura, Naka-gun, Ibaraki 319-1112, Japan*

⁴*School of Physics, Beihang University 100083, People's Republic of China*

⁵*Center for Computational Sciences, University of Tsukuba, 1-1-1, Tennodai Tsukuba, Ibaraki 305-8577, Japan*

(Dated: October 2, 2024)

In this study, we developed and tested various isospin symmetry-breaking (ISB) versions of the microscopic DJ16A interaction. Starting with the isospin symmetric DJ16A interaction, we introduced two different Coulomb interactions—Coulomb-CD and Coulomb-w/SRC—along with phenomenological charge symmetry breaking (CSB) and charge independence breaking (CIB) effects. We also considered CSB and CIB parts of the Argonne v18 (AV18) interaction. We examined two sets of interactions for each Coulomb interaction and employed these interactions to calculate b - and c -parameters of the isobaric multiplet mass equation for $|T_z| = 1/2$ and $|T_z| = 1$ nuclei across the sd -shell. Our results indicate that the DJ16A[†]+CD interaction provides the most accurate b -parameter predictions up to $A = 33$ mirror pairs. Additionally, we explored mirror energy differences (MEDs) in low-energy spectra around $A = 20$ and demonstrated that large MEDs are primarily associated with high occupancies of the $1s_{1/2}$ orbital. Furthermore, $E2$ transition strengths were calculated using all four DJ16A-based ISB interactions agreed with the experimental data, with minimal ISB effects observed on these transitions. Overall, the DJ16A[†]+CD interaction serves as a complementary set to the newly developed USD-family interactions, USDC, and USDCm and can be further tested for other mirror nuclei across the sd -shell to study nuclear structure properties and ISB effects in nuclear β -decay.

PACS numbers: 21.60.Cs, 21.30.Fe, 21.10.Dr, 27.20.+n

I. INTRODUCTION

Atomic nuclei are self-bound quantum many-body systems consisting of protons and neutrons collectively known as nucleons. Due to the similar masses and intrinsic spins of protons and neutrons, they were considered to be isospin doublets having different isospin projections [1, 2]. In nuclear physics, the isospin symmetry approximation provides an efficient way of developing nucleon-nucleon interactions and simplifying the solution of nuclear many-body problems. Also, the nuclear forces among the protons ($T_z = -1/2$) and the neutrons ($T_z = 1/2$) are the same within the isospin symmetry approximation. And, for such isospin symmetric nucleon-nucleon interactions, the energy spectra of mirror nuclei, whose protons and neutrons are exchanged, have degenerate excitation spectra. However, isospin symmetry is broken at the nuclear level mainly due to Coulomb interaction among the protons, the mass difference between the proton and the neutron, and the charge-dependent nature of nuclear force. Also, the experimental phase shifts showed that V_{nn} is almost 1 % larger than V_{pp} , resulting in the charge symmetry breaking (CSB), and V_{pn} is about 2.5 % larger than $(V_{nn} + V_{pp})/2$, resulting in charge independence breaking (CIB) of nuclear force. All these effects

result in the isospin symmetry breaking (ISB) at the nuclear level, and the origin of ISB in nuclear systems can be studied using different nuclear models such as the shell model [3–5] and density-functional theory [6, 7]. This work uses the shell model approach to study ISB effects in the sd -shell nuclei.

The ISB effects provide a way to test different nuclear models and can also help in understanding the nature of nucleon-nucleon forces. These effects are reflected in the isospin-mixing in nuclear states, correction factors needed in the study of β -decay [8, 9], and in some isospin-forbidden processes [10–12]. The mirror energy difference (MED) and triplet energy difference (TED) are two key quantities to understand ISB in the low-energy spectra of atomic nuclei, and both these quantities are sensitive to the Coulomb and charge-dependent part of an isospin-symmetry breaking Hamiltonian. For such ISB Hamiltonians, the degeneracy between the spectra of mirror pairs of nuclei is broken, resulting in a non-zero MED value. While the MEDs for medium mass nuclei in the fp -shell are relatively small (around 0.1 MeV) [13], for the lighter mass nuclei in the sd -shell can reach near to 1 MeV in some cases [14]. Usually, large MEDs are observed for mirror pairs whose proton-rich partner is near the proton drip line. In such cases, the proton $0d_{5/2}$ and $1s_{1/2}$ orbitals are loosely bound while they are deeply bound on the neutron-rich side. This is known as the Thomas-Ehrman (TE) shift [15, 16]. Accurate modeling of Coulomb and charge-dependent nuclear forces is

* praveen.srivastava@ph.iitr.ac.in

essential to explain the observed MEDs in mirror pairs of nuclei [17]. The MED and structure of loosely bound proton-rich *sd*-shell nuclei around $A = 20$ are discussed in Ref. [18]. The authors explained the need to reduce some of the two body matrix elements (TBME) to accommodate the weakly bound or unbound effect in such nuclei. The ISB effects within *sd*-shell nuclei and beyond are elaborated in Ref. [19] by taking into account short-range correlations to the Coulomb interaction and effective charge-dependent force of nuclear origin. Recently, two ISB interactions of USD-type [20–22] are available, namely USDC and USDI [23], to study ISB effects within the nuclear shell model. The ISB interaction USDC is utilized in Ref. [24] to study the contributions of isoscalar and isovector components to the $M1$ transitions of odd- A nuclei in the *sd*-shell. In Ref. [25], the b and c parameters of the isobaric multiplet mass equation (IMME) are calculated using valence space in-medium similarity renormalization group (VS-IMSRG) for $T = 1$ nuclei from $A = 10$ to 74 and observed a good agreement with the experimental data. In Refs. [26, 27], the MEDs in the low energy spectra of *sd*-shell nuclei are discussed using VS-IMSRG formalism. Also, in Refs. [28, 29], the same VS-IMSRG technique is used to study $E2$ transition strengths within the *sd*-shell nuclei, and it was observed that the $B(E2)$ values for VS-IMSRG show consistent underprediction compared to the experimental data. The VS-IMSRG technique and shell model calculations using ISB USD-family interactions have recently been applied to different nuclei in the *sd*-shell to study ISB effects [30–33].

Recently, in Ref. [34], we calculated the MEDs in the low-lying states of $|T_z| = 1/2$ mirror pair ($^{21}\text{Na} - ^{21}\text{Ne}$) within the no-core shell model (NCSM) formalism. However, due to the computational limitations, calculations were possible only up to $N_{max} = 4$ model space. In such a scenario, microscopic effective interactions based on the NCSM solutions of lower-mass nuclei can be useful [35, 36]. Additionally, ISB versions of such microscopic interactions would be beneficial for studying ISB effects across *sd*-shell nuclei, and they can serve as a complementary set of interactions to the newly developed USD-family interactions [23]. In this work, we have constructed the ISB versions for microscopic interaction DJ16A (monopole-modified version of DJ16 interaction) [37] to study the ISB effect in the low-energy spectra of $|T_z| = 1/2$ and $|T_z| = 1$ mirror pairs within the *sd*-shell.

This paper is organized as follows: In section II, we briefly describe NCSM with a core approach to developing microscopic effective *sd*-shell interaction along with different Coulomb interactions considered; section III is devoted to presenting the calculated results on IMME, low-energy spectra, and MEDs along with the $E2$ transition strengths. Finally, we summarize our work in section IV.

II. FORMALISM

The nuclear shell model stands as a cornerstone of our understanding of the nuclear structure, offering profound insights into various low-energy properties of atomic nuclei. Central to its framework is the employment of extensive diagonalization within a many-body harmonic oscillator basis. Given the rotational invariance of the nuclear force, it is advantageous to employ single-particle harmonic oscillator states characterized by well-defined quantum numbers: principal quantum number (n), azimuthal quantum number (l), total angular momentum (j), and its z-component (j_z). In the traditional shell model, the effective interactions among the valence nucleons are considered in a truncated model space instead of all nucleons being active. Those effective interactions are expressed in terms of SPEs and TBMEs for different truncated spaces are key ingredients of the shell model calculations.

In the early phase of the nuclear shell model, effective interactions were developed with perturbative approaches [38, 39]. Later, the phenomenological interactions for different model spaces become widely successful in reproducing low-energy spectroscopic data of nuclei in different mass regions [20–22, 40–44]. In the last two decades, the *ab initio* methods exhibited great progress, and those methods provide a way to use chiral interactions from effective field theory directly to study nuclear properties [45–48]. Additionally, using similarity transformations, the *ab initio* methods opened a new path to develop effective interactions for a particular valence space. Two such *ab initio* methods are the NCSM [45, 49–52] and VS-IMSRG [46, 47] methods. Our present work aims to utilize effective interactions developed using the former *ab initio* method.

In Ref. [35], a new non-perturbative way of developing effective interactions was proposed starting from *ab initio* NCSM wavefunctions of a few selected lower p -shell nuclei. The same technique was recently used to develop effective microscopic interactions for *sd*-shell, namely JISP16 [36], N3LO [36], and DJ16 [37]. These effective interactions were derived from the original interactions [53–55] using the *ab initio* NCSM wave function and Okubu-Lee-Suzuki (OLS) [56] technique. Some of these microscopic interactions have recently been applied to *sd* shell nuclei in Refs. [57–60] in order to study different structure properties.

Considering only NN interaction, the NCSM Hamiltonian can be written as

$$H_A = T_{rel} + V = \frac{1}{A} \sum_{i < j}^A \frac{(\vec{p}_i - \vec{p}_j)^2}{2m} + \sum_{i < j}^A V_{ij}^{NN}, \quad (1)$$

where T_{rel} is the relative kinetic energy and V_{ij}^{NN} is the NN interaction containing nuclear part as well as Coulomb part. The Equation 1 is in a relative coordinate system, and it is converted to the harmonic oscillator ba-

sis by adding the center of mass (H_{CM}) to the original Hamiltonian, H_A having the form

$$H_A^\Omega = H_A + H_{c.m.} = \sum_{i=1}^A \left[\frac{p_i^2}{2m} + \frac{1}{2} m \Omega^2 r_i^2 \right] + \sum_{i<j}^A \left[V_{NN,ij} - \frac{m\Omega^2}{2A} (r_i - r_j)^2 \right]. \quad (2)$$

Considering an OLS transformation to the above Hamiltonian, at 2-body cluster approximation, primary Hamiltonians for $A = 18$ systems were constructed. Then the NCSM calculations were performed for ^{18}F (at $N_{max} = 4$, $\hbar\Omega = 14$ MeV), and 28 eigenstates dominated by $N = 0$ components were considered in constructing a secondary OLS transformation to the sd -model space. Additionally, the NCSM calculations were performed for ^{16}O to obtain the core energy and for ^{17}O and ^{17}F to get neutron and proton SPEs. Finally, subtracting the core plus SPEs from the effective Hamiltonian for ^{18}F resulted in the TBMEs for effective sd -shell interaction, DJ16 [37]. The DJ16 interaction given in Ref. [37] was obtained from the NCSM calculations considering charge symmetry and charge independence of nuclear force. However, a full-charge dependent version for this effective interaction is possible by deriving effective interactions for ^{18}O and ^{18}Ne , separately for the V_{nn} and V_{pp} parts, respectively [61].

This work follows a different route to construct ISB versions of microscopic sd -shell effective interaction corresponding to monopole-modified DJ16 interaction (DJ16A). Starting with the isospin symmetric interaction DJ16A, we intended to obtain suitable ISB versions of this interaction having the form:

$$H = H_0 + H_C + H_{INC}, \quad (3)$$

where H_0 is the isospin-conserving interaction, and for our case, it is the DJ16A interaction. H_C and H_{INC} are Coulomb interaction and isospin non-conserving part of nuclear force, respectively. This work employed two sets of Coulomb interactions from Ref. [23]: Coulomb-CD and Coulomb-w/SRC. In Coulomb-CD, the TBMEs for Coulomb interaction were calculated using a harmonic oscillator basis, and the TBMEs are dependent on mass as $\sim A^{-1/6}$. On the other hand, in Coulomb-w/SRC, the short-range correlations (SRC) given by Miller and Spencer [62] were considered as a correction factor. It is well known that the Coulomb interaction is not the only factor responsible for energy splitting in an isobaric multiplet, and it is known as the Nolen-Schiffer anomaly [63]. The charge-dependent nuclear force needs to be considered along with the Coulomb interaction to explain such ISB effects in atomic nuclei. While using USDC and USDCm interactions, an increase of the $V_{pn}(T=1)$ part by 2.2 % and 0.8 %, respectively, are mentioned in Ref. [23]. However, instead of increasing the $V_{pn}(T=1)$

part by a certain amount, the charge symmetry breaking (CSB) and charge independence breaking (CIB) effects can be taken into account in addition to the Coulomb interaction.

In this work, we aim to test the effect of CSB and CIB interactions in the low-energy spectra of sd -shell nuclei. Once the CSB and CIB interactions are considered, the V_{pp} , V_{nn} , and $V_{pn}(T=1)$ parts of the isospin symmetric interactions get modified as:

$$\begin{aligned} V_{pp} &= V_0 + V_{CSB}/2 + V_{CIB}/3 \\ V_{nn} &= V_0 - V_{CSB}/2 + V_{CIB}/3 \\ V_{pn}(T=1) &= V_0 - 2V_{CIB}/3 \end{aligned}$$

Here, V_0 is the isospin symmetric part of the interaction. In addition to modifying TBMEs, the V_{CSB} also modifies the proton SPEs compared to the neutron SPEs. On the other hand, V_{CIB} does not affect the proton SPEs. For that, firstly, we consider phenomenological CSB and CIB interactions from Ref. [64] that reproduce the experimental differences in scattering lengths and effective ranges. The interactions having the Yukawa form, $V_0 e^{-r/R_0}/(r/R_0)$ with radial cutoff at 0.45 fm are used for phenomenological CSB and CIB interactions. We call them CSB^Y and CIB^Y interactions, respectively. For the CSB^Y , the Coulomb displacement energy (CDE) for the ^{17}F - ^{17}O pair is obtained to be ~ 190 keV [64], which is larger than that of 100 keV obtained by the ρ - ω and π - η meson exchange interactions [65]. Secondly, we consider the CSB and CIB parts of the AV18 interaction [66] with a radial cut-off at 0.7 fm for the short-range components, and we call them CSB^{AV18} and CIB^{AV18} , respectively. CSB^{AV18} is rather small: the CDE for the ^{17}F - ^{17}O pair obtained by the CSB^{AV18} is as small as 65 keV compared to the empirical value of 135 (109) keV evaluated for Woods-Saxon (Hartree-Fock) wave functions [65]. The CIB interaction of AV18 consists of the one-pion-exchange potential (OPEP) components with different masses for charged and neutral pions and short-range terms. The OPEP contains the short-range correlation with exponential cut-off while the short-range terms are sensitive to the radial cut-off. For the present choice of the cut-off at 0.7 fm for the short-range components, the dominant contributions to CIB^{AV18} come from the OPEP.

The addition of Coulomb and CSB interactions to the isospin-conserving interaction shifts the single-particle energies (SPE) of proton orbitals with respect to the corresponding neutron SPEs along with a reduction in the magnitude of proton-proton two-body matrix elements (TBME) in most cases. However, the inclusion of CIB interaction shifts the proton and neutron TBMEs by the same amount. We consider four sets of interactions for each Coulomb interaction:

(i) DJ16A + CD (w/SRC) combines isospin symmetric DJ16A interaction with a Coulomb part without considering the CSB and CIB effects,

TABLE I. The SPEs for proton orbitals corresponding to different ISB interactions are shown. The Coulomb SPEs for DJ16A + CD (w/SRC) and DJ16A + CSB^Y + CD (w/SRC) are taken from [23].

Interaction	$0d_{5/2}$	$1s_{1/2}$	$0d_{3/2}$
DJ16A + CD	-0.3508	0.2764	5.6377
DJ16A + CSB ^Y + CD	-0.1488	0.5268	5.8397
DJ16A [†] + CD	-0.3828	-0.0650	5.7415
DJ16A* + CD	-0.3828	0.4200	5.7415
DJ16A + w/SRC	-0.2978	0.1159	5.5631
DJ16A + CSB ^Y + w/SRC	-0.0958	0.3663	5.7651
DJ16A [†] + w/SRC	-0.3828	-0.1220	5.7415
DJ16A* + w/SRC	-0.3828	0.3350	5.7415
USDCm	-0.3836	0.1749	5.3529

- (ii) DJ16A + CSB^Y + CD (w/SRC) additionally combine CSB^Y interaction with DJ16A + CD (w/SRC),
- (iii) DJ16A[†] + CD (w/SRC) takes into account Coulomb, CSB^Y and CIB^Y interactions and it is tuned to reproduce experimental $b(A = 17)$, $b(A = 18)$ and $c(A = 18)$, and
- (iv) DJ16A* + CD (w/SRC) is same as (iii) interactions with replacement of CSB^Y and CIB^Y by CSB^{AV18} and CIB^{AV18}.

The proton SPEs for these eight sets of interactions are shown in Table I. Explanations for the determination of the proton SPEs are given in section III A. In order to understand the impact of the Coulomb and CSB TBMEs in modifying the V_{pp} part of the original isospin-symmetric Hamiltonians, we tabulated $|V_{pp}/V_{nn}|$ for a few TBMEs involving only $0d_{5/2}$ and $1s_{1/2}$ orbitals corresponding to DJ16A + Coulomb, DJ16A + CSB + Coulomb, DJ16A[†] + Coulomb, and DJ16A* + Coulomb in Table II. In the fourth column of the table, we added $|V_{pp}/V_{nn}|$ corresponding to the same set of TBMEs for USDCm interaction. Additionally, the suggested reduction factor for the V_{pp} part of USDB interactions is also shown in the fifth column of the table taken from [18]. The table shows that the Coulomb and Coulomb + CSB reduces proton-proton TBMEs by a factor in most cases, while CIB shifts pp and nn TBMEs by the same amount.

III. RESULTS AND DISCUSSIONS

A. Isobaric multiplet mass equation:

The IMME holds the signature of ISB in atomic nuclei. As demonstrated by Wigner [67], the mass difference of isobaric analog states within an isospin multiplet can be expressed as a quadratic form of T_z as:

$$ME(A, T, T_z) = a + bT_z + cT_z^2 \quad (4)$$

where ME is mass excess. The a and b parameters for $|T_z| = 1/2$ doublets can be written as:

$$\begin{aligned} a &= ME(T_z = 1/2) + ME(T_z = -1/2) \\ b &= ME(T_z = 1/2) - ME(T_z = -1/2) \end{aligned}$$

The a , b , and c parameters for $|T_z| = 1$ triplets are written as:

$$\begin{aligned} a &= ME(T_z = 0) \\ b &= ME(T_z = 1) - ME(T_z = -1) \\ c &= [ME(T_z = 1) + ME(T_z = -1)]/2 - ME(T_z = 0) \end{aligned}$$

In this work, we started with the isospin-symmetric DJ16A interaction from Ref. [37]. We then added two different Coulomb interactions (Coulomb-CD and Coulomb-w/SRC) from Ref. [23] to get two ISB interactions: DJ16A + CD and DJ16A + w/SRC and calculated the g.s. b -parameters for $|T_z| = 1/2$ and 1 mirror pairs. Then, those results were compared with the experimental b parameter extracted using the mass-excess data taken from [68]. Additionally, we incorporated the phenomenological CSB effects on the TBMEs of DJ16A + CD and DJ16A + w/SRC to have two additional sets of interactions: DJ16A + CSB^Y + CD and DJ16A + CSB^Y + w/SRC. The proton SPEs for both sets are shown in Table I. The calculated $b(A = 17)$ corresponding to DJ16A + CD and DJ16A + w/SRC are -3.575 and -3.628 MeV, respectively compared to the experimental $b(A = 17)$ of -3.543 MeV. The CSB effects modify these values to -3.777 and -3.830 MeV, respectively. On the other hand, the $b(A = 18)$ for DJ16A + CD and DJ16A + w/SRC interactions are -3.810 and -3.827 MeV, which are close to the experimental value of -3.833 MeV. However, $b(A = 18)$ for DJ16A + CSB^Y + CD and DJ16A + CSB^Y + w/SRC interactions are -4.149 and -4.168 MeV, respectively. From these discussions, it can be concluded that the CSB effects shift the calculated $b(A = 17)$ and $b(A = 18)$ away from the experimental data. So, we aim to modify the proton SPEs for both DJ16A + CSB^Y + CD and DJ16A + CSB^Y + w/SRC in order to reproduce experimental $b(A = 17)$ and $b(A = 18)$. The steps are as follows:

- (i) Firstly, we modify the proton SPEs for both the interactions with the CSB contributions comparing the experimental binding energies and spectra of ¹⁷O and ¹⁷F, which reproduce the experimental $b(A = 17)$, exactly.
- (ii) Secondly, we further tuned the proton SPEs of $1s_{1/2}$ orbital for DJ16A + CSB^Y + CD and DJ16A + CSB^Y + w/SRC separately to reproduce experimental $b(A = 18)$. Finally, we focused on reproducing the experimental $c(A = 18)$ once phenomenological CIB effects were also included. The $c(A = 18)$ for DJ16A + CSB^Y + CD and DJ16A + CSB^Y + w/SRC interactions with tuned proton SPEs were 435 and 448 keV, respectively, compared to the experimental $c(A = 18) = 352$ keV. In order to match the calculated $c(A = 17)$ with the experimental data, we reduced CIB^Y strength by a factor of 0.35 and

TABLE II. The $|V_{pp}/V_{nn}|$ for a few TBMEs involving only $0d_{5/2}$ and $1s_{1/2}$ orbitals corresponding to DJ16A + Coulomb, DJ16A + CSB^Y + Coulomb, DJ16A[†]+Coulomb, DJ16A*+Coulomb and USDCm [23] are shown. The suggested reduction factor for the V_{pp} part of USDB* is taken from [18].

TBME ($\langle ij V kl\rangle_{JT}$)	DJ16A + CD	DJ16A + w/SRC	USDCm	USDB*
$\langle(1s_{1/2}^2) V (1s_{1/2})^2\rangle_{01}$	0.80	0.79	0.73	0.68
$\langle 1s_{1/2}0d_{5/2} V 1s_{1/2}0d_{5/2}\rangle_{31}$	1.48	1.51	1.58	0.78
$\langle 1s_{1/2}0d_{5/2} V 1s_{1/2}0d_{5/2}\rangle_{21}$	0.62	0.59	0.51	0.84
$\langle(0d_{5/2})^2 V (1s_{1/2})^2\rangle_{01}$	0.98	0.98	0.94	0.80
$\langle 1s_{1/2}0d_{5/2} V (0d_{5/2})^2\rangle_{21}$	0.96	0.95	0.89	0.87
TBME ($\langle ij V kl\rangle_{JT}$)	DJ16A + CSB ^Y + CD	DJ16 + CSB ^Y + w/SRC	USDCm	USDB*
$\langle(1s_{1/2}^2) V (1s_{1/2})^2\rangle_{01}$	0.73	0.72	0.73	0.68
$\langle 1s_{1/2}0d_{5/2} V 1s_{1/2}0d_{5/2}\rangle_{31}$	1.52	1.55	1.58	0.78
$\langle 1s_{1/2}0d_{5/2} V 1s_{1/2}0d_{5/2}\rangle_{21}$	0.57	0.55	0.51	0.84
$\langle(0d_{5/2})^2 V (1s_{1/2})^2\rangle_{01}$	0.93	0.93	0.94	0.80
$\langle 1s_{1/2}0d_{5/2} V (0d_{5/2})^2\rangle_{21}$	0.90	0.90	0.89	0.87
TBME ($\langle ij V kl\rangle_{JT}$)	DJ16A [†] + CD	DJ16A [†] + w/SRC	USDCm	USDB*
$\langle(1s_{1/2}^2) V (1s_{1/2})^2\rangle_{01}$	0.73	0.72	0.73	0.68
$\langle 1s_{1/2}0d_{5/2} V 1s_{1/2}0d_{5/2}\rangle_{31}$	1.52	1.55	1.58	0.78
$\langle 1s_{1/2}0d_{5/2} V 1s_{1/2}0d_{5/2}\rangle_{21}$	0.57	0.54	0.51	0.84
$\langle(0d_{5/2})^2 V (1s_{1/2})^2\rangle_{01}$	0.93	0.93	0.94	0.80
$\langle 1s_{1/2}0d_{5/2} V (0d_{5/2})^2\rangle_{21}$	0.90	0.90	0.89	0.87
TBME ($\langle ij V kl\rangle_{JT}$)	DJ16A* + CD	DJ16A* + w/SRC	USDCm	USDB*
$\langle(1s_{1/2}^2) V (1s_{1/2})^2\rangle_{01}$	0.77	0.76	0.73	0.68
$\langle 1s_{1/2}0d_{5/2} V 1s_{1/2}0d_{5/2}\rangle_{31}$	1.52	1.55	1.58	0.78
$\langle 1s_{1/2}0d_{5/2} V 1s_{1/2}0d_{5/2}\rangle_{21}$	0.59	0.56	0.51	0.84
$\langle(0d_{5/2})^2 V (1s_{1/2})^2\rangle_{01}$	0.97	0.97	0.94	0.80
$\langle 1s_{1/2}0d_{5/2} V (0d_{5/2})^2\rangle_{21}$	0.95	0.94	0.89	0.87

0.29 for DJ16A + CSB^Y + CD and DJ16A + CSB^Y + w/SRC. These final sets are denoted as DJ16A[†] + CD and DJ16A[†] + w/SRC in the rest of the paper. On the other hand, while using CSB and CIB effects from AV18 interaction the proton SPEs are modified as discussed earlier. However, no reduction of the CIB part is done like before, and we get two additional sets of interactions: DJ16A* + CD and DJ16A* + w/SRC. The proton SPEs for these final set of ISB interactions were shown in Table I.

We now compare the performance of these four sets of interactions in reproducing the experimental b -parameters of a few mirror pairs across the sd -shell. We use root mean square deviation (rms) of b -parameters for that purpose defined as:

$$b_{rms} = \sqrt{\frac{1}{N} \sum_i^N (b_{exp}^i - b_{th}^i)^2}. \quad (5)$$

Here, $N = 12$ for $T_z = 1/2$ doublets ($A = 17$ to 39), and $N = 11$ for $T_z = 1$ triplets ($A = 18$ to 38). The b_{rms} of the g.s. of $|T_z| = 1/2$ and $|T_z| = 1$ nuclei were calculated separately for DJ16A[†] + CD, DJ16A[†] + w/SRC, DJ16A* + CD, and DJ16A* + w/SRC and those results are compared to the USDCm results.

The DJ16A interaction, combined with two different Coulomb interactions and CSB and CIB effects, can reproduce the correct ground states of $A = 17$ to 39,

$|T_z| = 1/2$ doublets with the exceptions of $A = 25$ and 27 nuclei. In the case of (²⁵Mg - ²⁵Al), $5/2^+$ is the g.s. and the calculated results with DJ16A[†] + Coulomb interactions show $1/2^+$ as the g.s. On the other hand, for the case of $A = 27$ pair, the g.s. of the proton-rich nucleus (²⁷Si) is correctly reproduced by all DJ16A-based interactions. However, for the neutron-rich partner (²⁷Al), it was found to be $3/2^+$ with a small separation between the g.s. and the first excited state ($5/2^+$). Based on the binding energies of g.s. with respect to ¹⁶O core, the b parameters are calculated for each pair of $|T_z| = 1/2$ doublets. The experimental and calculated b parameters are compared in the first panel of Figure 1. From the figure, it can be seen that the DJ16A[†]+CD and DJ16A*+CD mimic the experimental b more closely up to $A = 33$, and after that, the USDCm and DJ16A*+CD show slightly better results than the other. The b_{rms} values for DJ16A[†]+CD and DJ16A*+CD are 75, and 93 keV, respectively, while considering all the g.s. of $A = 17$ to 33 doublets. The b_{rms} value for the USDCm interaction corresponding to the same set of nuclei is 92 keV. In the second panel of Figure 1, calculated Δb values (here, Δb for mass number A is calculated by taking the differences between $b(A+2)$ and $b(A)$) corresponding to DJ16A[†]+CD, DJ16A[†]+w/SRC, DJ16A*+CD, DJ16A*+w/SRC, and USDCm are compared to the experimental data. The figure shows that DJ16A-based interactions along with the USDCm, can reproduce the experimental staggering

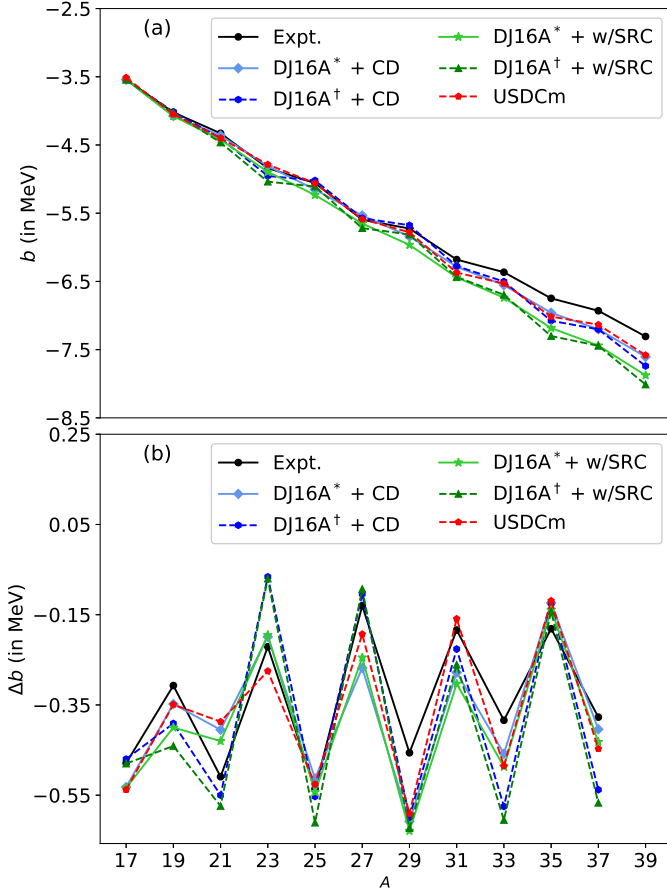


FIG. 1. (a) The calculated b parameters using DJ16A*+CD, DJ16A†+CD, DJ16A*+w/SRC, DJ16A†+w/SRC and USDCm are compared with the experimental data collected from Ref. [68] for $|T_z| = 1/2$ pairs, (b) the calculated Δb parameters using the same sets of interactions are compared with the experimental data collected from Ref. [68]. The Δb for A is calculated by taking the differences between the b values of $A + 2$ and A nuclei.

pattern of Δb correctly.

Similar to the case of $|T_z| = 1/2$ pairs, the calculated and experimental b parameters for $|T_z| = 1$ are compared in Figure 2. The DJ16A interaction combined with two different coulomb interactions and CSB and CIB effects, can reproduce the g.s. of $|T_z| = 1$ pairs from $A = 18$ to 38 except for $A = 24$ and 28 pairs. For the case of $A = 24$ pairs, 4_1^+ is the g.s. and calculated results with DJ16A-based interactions showed 1_1^+ as the g.s. The calculated results with USDCm also showed 1_1^+ as the g.s. of $A = 24$ mirror pair. On the other hand, all five interactions showed 2_1^+ as the g.s. of ($^{28}\text{P} - ^{28}\text{Al}$) mirror pair instead

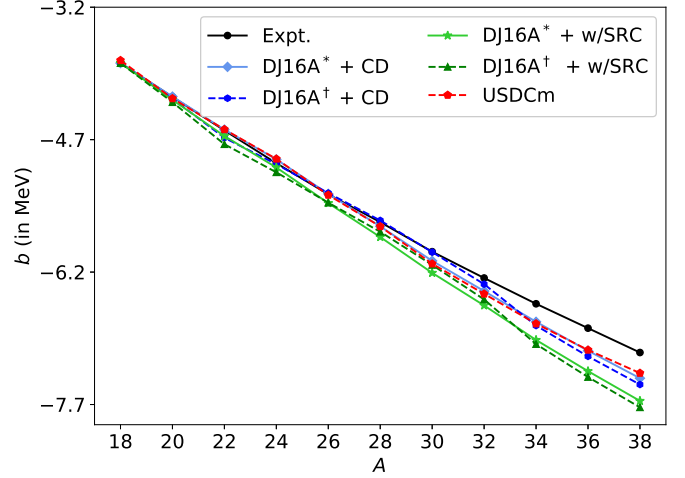


FIG. 2. The calculated b parameters using DJ16A†+CD, DJ16A†+w/SRC, and USDCm are compared with the experimental data collected from Ref. [68] for $|T_z| = 1$ pair.

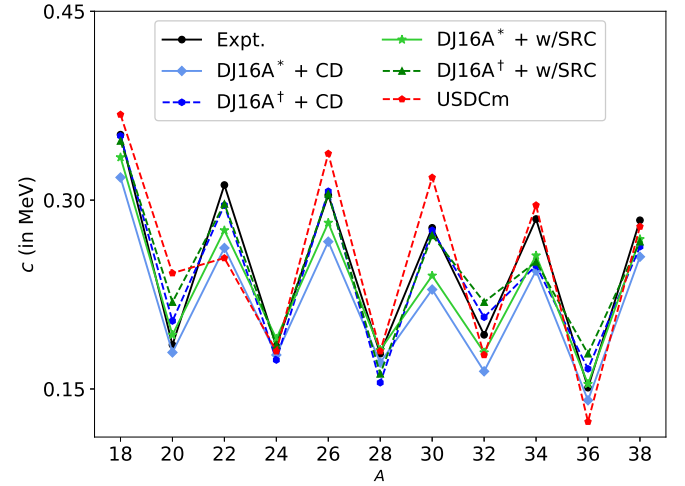


FIG. 3. The calculated c parameters using DJ16A†+CD, DJ16A†+w/SRC, and USDCm are compared with the experimental data collected from Ref. [68] for $|T_z| = 1$ triplet.

of the experimental g.s. (3_1^+). From the figure, it can be seen that the calculated b -parameters using DJ16A†+CD and DJ16A*+CD are closer to experimental data up to $A = 32$ compared to the other interactions. The b_{rms} values of DJ16A†+CD, DJ16A*+w/SRC, and USDCm are 40, 68, and 84 keV, respectively, up to $A = 32$. Based on the b_{rms} values of the g.s. of $|T_z| = 1/2$ and $|T_z| = 1$ nuclei across sd -shell, the DJ16A†+CD and DJ16A*+CD interactions showed low b_{rms} up to $A = 33$ mirror pair.

Additionally, we calculated the c -parameters for the $|T_z| = 1$ nuclei across sd -shell. Firstly, we calculated

the c -parameters for DJ16A+Coulomb, and those results are significantly less than the experimental c -parameters suggesting the need for including the CIB effects. For example, both DJ16A+CD and DJ16A+CSB+CD result in $c(A = 18) = 254$ keV instead of the experimental value of 352 keV. Once we added the CIB^Y effects, the calculated $c(A = 18)$ became 557 and 571 keV, respectively, for DJ16A+CD and DJ16A+w/SRC, along with the phenomenological CSB and CIB interactions. If the tuned proton SPEs are used instead of the original ones, the $c(A = 18)$ become 435 and 448 keV, respectively which are still higher than the experimental data. It is well known that the c parameters are proportional to the CIB strength, so in order to reproduce the experimental $c(A = 18)$, we focused on reducing the CIB^Y strength by some particular amount. On multiplying the original CIB^Y TBMEs by a factor of 0.35 and 0.29 along with using the tuned proton SPEs, we got DJ16A[†]+CD and DJ16A[†]+w/SRC and the calculated $c(A = 18)$ for these two interactions are close to the experimental data. While using CSB^{AV18} and CIB^{AV18} instead of the phenomenological ones, the tuned proton SPEs are considered as the earlier case without reducing the strength of CIB^{AV18}. In Figure 3, we showed a comparison between the calculated and experimental c -parameters. From the figure, it can be seen that the calculated c parameters are able to reproduce the staggering pattern of the experimental data.

B. Mirror energy differences

The effect of isospin symmetry breaking can also be seen in the low-energy spectra of mirror nuclei. The MED provides an estimation of the ISB in low-energy spectra, and it is defined as:

$$MED_J = E_J(T_z = -T) - E_J(T_z = +T). \quad (6)$$

Here, E_J are the excitation energies of isobaric analog states with angular momentum J in a mirror pair with $T_z = \pm T$. Among the eleven $|T_z| = 1/2$ doublets, we selected (¹⁹Ne - ¹⁹F) and (²¹Na - ²¹Ne) mirror pairs whose one or more states show large MED (more than 200 keV). For the $A = 19$ pair, the $11/2_1^+$ shows MED more than 200 keV, and in the case of $A = 21$ pairs, three states $1/2_1^+$, $5/2_3^+$ and $3/2_2^+$ show MED more than 200 keV. Additionally, we select two pairs of $|T_z| = 1$ nuclei: (¹⁸Ne - ¹⁸O) and (²⁰Na - ²⁰F) for which large MEDs are observed. The spectra and MEDs corresponding to these pairs of nuclei are shown in Figures 4-11.

¹⁹Ne/¹⁹F: The low-energy spectra of (¹⁹Ne - ¹⁹F) mirror pair is shown in Figure 4. The shell model calculations were performed using four DJ16A-based ISB interactions, namely DJ16A* + CD, DJ16A[†] + CD, DJ16A* + w/SRC, and DJ16A[†] + w/SRC, and recently developed USDCm interactions. The calculated spectra follow the correct ordering as the experimental data up to the

third excited state ($9/2_1^+$). Experimentally, the first excited state ($5/2_1^+$) of ¹⁹Ne and ¹⁹F are at 0.238 and 0.197 MeV, respectively. While the USDCm interaction shows excitation energies of $5/2_1^+$ state around 60 keV for both nuclei, the DJ16A[†] + Coulomb interactions show excitation energies of more than 400 keV. On the other hand, DJ16A* + Coulomb interactions show the excitation energy of the same state around 370 keV. Interestingly, all five interactions employed in this work show the $3/2_2^+$ states at higher energy (around 7 MeV), contrary to the experimental excitation energies of 4 MeV. Experimentally, the un-confirmed $11/2^+$ state of ¹⁹Ne is found to be at 6291.6(9) keV [69], and its mirror counterpart in ¹⁹F is observed at 6500.0(9) [70] keV providing a MED of -208.4(18) keV for this particular state. The calculated MEDs in the low-energy spectra of (¹⁹Ne - ¹⁹F) mirror pair corresponding to DJ16A*+CD, DJ16A[†]+CD, DJ16A*+w/SRC, DJ16A[†]+w/SRC, and USDCm are compared to the experimental data in the lower panel of Figure 6. The calculated MED of $11/2^+$ using USDCm is obtained to be -227 keV, whose strength is slightly more than the experimental MED. On the contrary, the MEDs of the same state corresponding to the DJ16A[†]+CD and DJ16A[†]+w/SRC are -320 and -339 keV, respectively. On the other hand, the MEDs of the same state corresponding to DJ16A*+CD and DJ16A*+w/SRC are -95 and -117 keV, respectively, whose strengths are less than the experimental data.

To understand the ISB effects in the low energy spectra clearly, the average occupancies of single-particle orbitals corresponding to DJ16A[†]+CD, DJ16A[†]+w/SRC, and USDCm are shown in the first, second, and third panels of Figure 6 along with the calculated and experimental MEDs in the fourth panel. The average occupancies of valence proton orbitals for the proton-rich nucleus (¹⁹Ne) and valence neutron orbitals of the neutron-rich nucleus (¹⁹F) are shown in the occupancy plots. Up to the third excited state ($9/2_1^+$), where valence proton and neutron occupancies are almost the same and dominated by the occupancies of valence $0d_{5/2}$ orbitals for all three interactions, resulting in small MEDs for those states. However, the $3/2_2^+$ state for USDCm interaction possesses the largest deviation (261 keV) between the experimental and calculated MEDs. The DJ16A[†]-based interactions also show large deviations around 240 keV for the same state. This difference is enhanced by the relatively large occupancy of proton $1s_{1/2}$ in ¹⁹Ne compared to neutron $1s_{1/2}$ occupancies of its mirror counterpart. Additionally, $5/2_2^+$, $13/2_1^+$, $5/2_3^+$ and $1/2_3^+$ states for USDCm also show large deviation (around 150 keV or more) from the experimental MEDs. While these large MED deviations in the case of $5/2_2^+$, $5/2_3^+$ and $1/2_3^+$ states can be attributed to the large occupancies of $1s_{1/2}$ orbitals, the substantial occupancies of $0d_{5/2}$ orbital could be responsible for large deviation of MED related to $13/2_1^+$ state as it has null contributions from $1s_{1/2}$ orbitals. Both of the DJ16A[†]-based interactions show fewer deviations compared to the USDCm for $5/2_2^+$

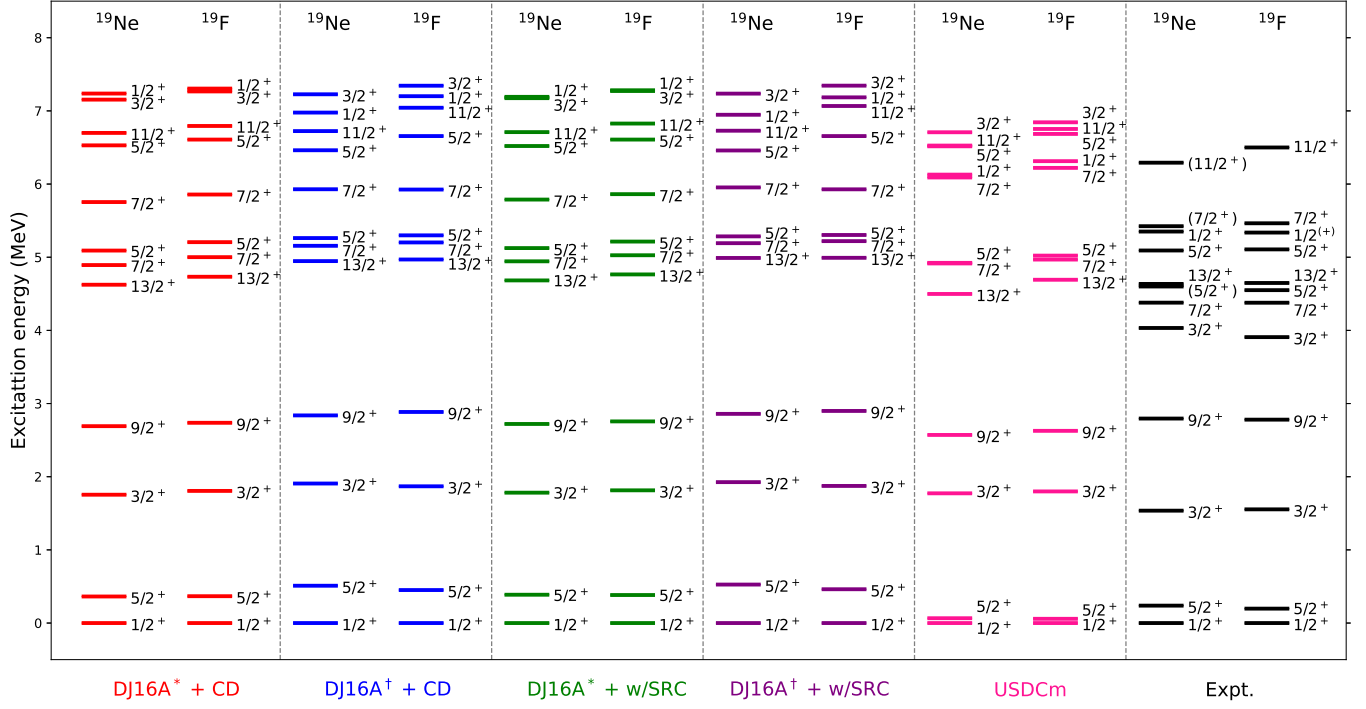


FIG. 4. Calculated low-energy spectra of $|T_z| = 1/2$ mirror pair ($^{19}\text{Ne} - ^{19}\text{F}$) using DJ16A*+CD, DJ16A†+CD, DJ16A*+w/SRC, DJ16A†+w/SRC and USDCm interactions are compared to the experimental data [70].

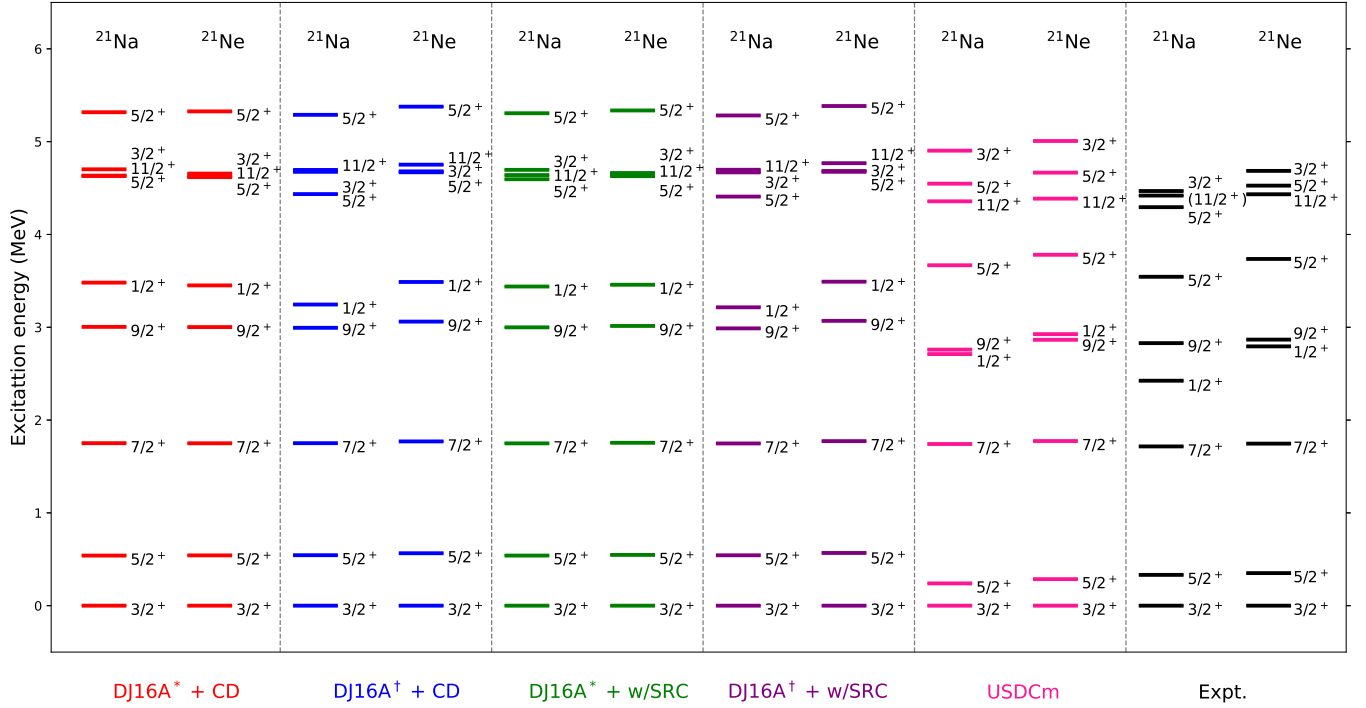


FIG. 5. Calculated low-energy spectra of $|T_z| = 1/2$ mirror pair ($^{21}\text{Na} - ^{21}\text{Ne}$) using DJ16A*+CD, DJ16A†+CD, DJ16A*+w/SRC, DJ16A†+w/SRC and USDCm interactions are compared to the experimental data [70].

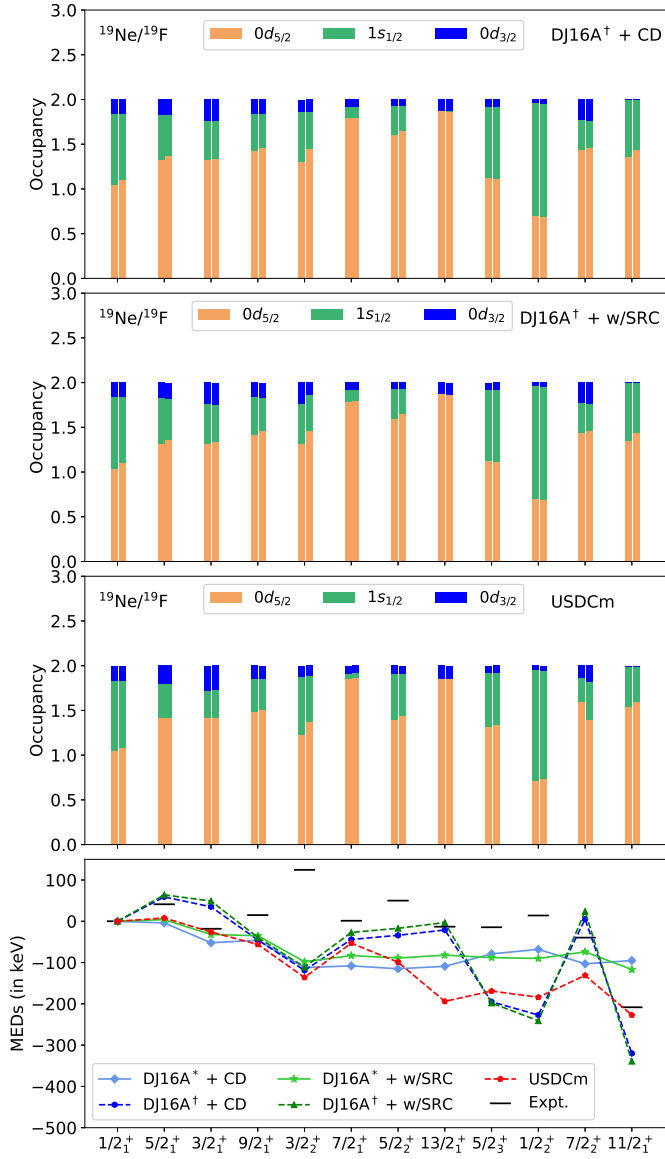


FIG. 6. Calculated average single orbital occupancies and MEDs for low-lying states of mirror pair ($^{19}\text{Ne} - ^{19}\text{F}$), using DJ16A † +CD, DJ16A † +w/SRC and USDCm interactions are shown. The displayed average occupancies correspond to the valence protons and neutrons in the respective mirror pair.

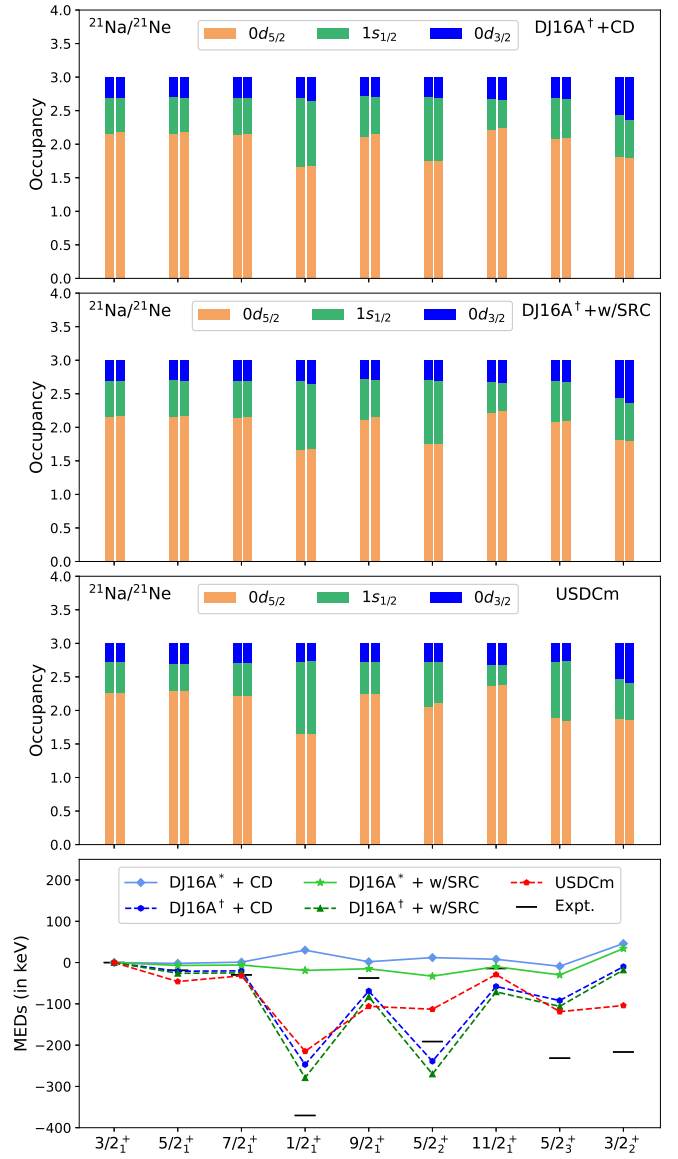


FIG. 7. Calculated average single orbital occupancies and MEDs for low-lying states of mirror pair ($^{21}\text{Na} - ^{21}\text{Ne}$), using DJ16A † +CD, DJ16A † +w/SRC and USDCm interactions are shown. The displayed average occupancies correspond to the valence protons and neutrons in the respective mirror pair.

and $13/2_1^+$ states. On the other hand, calculated MEDs of $5/2_3^+$ and $1/2_3^+$ states corresponding to $\text{DJ16A}^\dagger+\text{CD}$ and $\text{DJ16A}^\dagger+\text{w/SRC}$ show more deviation from the experimental data compared to the USDCm interaction. The USDCm interaction is able to reproduce close to the experimental MED of $11/2_1^+$ state compared to the other two interactions. The large occupancies of $1s_{1/2}$ orbital are solely responsible for this large MED as $0d_{3/2}$ occupancies are negligibly small for all three interactions. On the other hand, both of the DJ16A^* -based interactions show almost constant MEDs for all the states above $9/2_1^+$.

$^{21}\text{Na}/^{21}\text{Ne}$: The calculated low-energy spectra of ($^{21}\text{Na} - ^{21}\text{Ne}$) mirror pair is shown in Figure 5 along with the experimental data. All four DJ16A -based interactions employed in this work are able to reproduce the correct ordering up to the second excited state ($7/2_1^+$). However, the ordering of the $1/2_1^+$ and $9/2_1^+$ is reversed for those microscopic interactions compared to the experimental data. For USDCm interactions, the $1/2_1^+$ and $9/2_1^+$ states are obtained to be close-lying states with an average separation of 55 keV, and for the case of neutron-rich mirror partner, the ordering of these two states is reversed. While the calculated excitation energies of $5/2_2^+$ states using USDCm interaction are comparable to the experimental excitation energies, the DJ16A -based interactions show the excitation energies of both $5/2_2^+$ and $5/2_3^+$ around 0.9 MeV higher than the experimental data.

In Figure 7, a comparison between the calculated and experimentally observed MEDs is shown (fourth panel) along with the single orbital average occupancies of valence nucleons corresponding to $\text{DJ16A}^\dagger+\text{CD}$ (first panel), $\text{DJ16A}^\dagger+\text{w/SRC}$ (second panel), and USDCm (third panel) interactions. Among the nine low-lying states of the $A = 21$ mirror pair, four states: $1/2_1^+$, $5/2_2^+$, $5/2_3^+$, and $3/2_2^+$ exhibit large MEDs close to -200 keV or greater. While the MEDs for the $5/2_2^+$, $5/2_3^+$, and $3/2_2^+$ states are around -200 keV, the $1/2_1^+$ state has a significantly larger MED of -370.37(43) keV.

While the calculated MED of $5/2_2^+$ using $\text{DJ16A}^\dagger+\text{CD}$ and $\text{DJ16A}^\dagger+\text{w/SRC}$ interactions overpredicted the experimental data by a few keVs, the calculated MEDs for USDCm showed underprediction for the same. The experimental MEDs of $5/2_3^+$ and $3/2_2^+$ states are -231.54(84) and -216.63(85) keV, and the calculated MEDs corresponding to USDCm ($\text{DJ16A}^\dagger+\text{w/SRC}$) are -119 (-106) and -104 (-18) keV, respectively. The calculated MEDs using $\text{DJ16A}^\dagger+\text{CD}$ interaction for these two states, even more, underpredict the experimental data. Similarly, the MEDs obtained for $1/2_1^+$ state corresponding to $\text{DJ16A}^\dagger+\text{CD}$, $\text{DJ16A}^\dagger+\text{w/SRC}$, and USDCm are -247, -279, and -215 keV, respectively, compared to the experimental MED of -370.37(43) keV. Though relatively large occupancies of $1s_{1/2}$ valence orbitals are responsible for theoretically observed MEDs more than -200 keV, the calculated MEDs of the $1/2_1^+$ state are still away from the experimental data. For the case of $1/2_1^+$ obtained using the USDCm interaction, the occupancies of $1s_{1/2}$ valence

orbital are almost the same as the other two interactions. However, the USDCm showed the MED of this state to be smaller than predicted by DJ16A -based interaction suggesting a weak ISB effect of the USDCm interaction compared to the other two interactions. Contrary to the above results, the DJ16A^* -based interactions show almost constant MEDs in the range 0 to -50 keV for all states.

$^{18}\text{Ne}/^{18}\text{O}$: In Figure 8, the calculated energy spectra of $|T_z| = 1$ mirror pair ($^{18}\text{Ne} - ^{18}\text{O}$) is compared to the experimental data. The $\text{DJ16A}^\dagger+\text{CD}$ and $\text{DJ16A}^\dagger+\text{w/SRC}$ interactions were able to reproduce the correct ordering of low-lying states for the proton-rich nucleus, ^{18}Ne . The 0_2^+ and 2_2^+ states of ^{18}Ne are obtained to be degenerate for $\text{DJ16A}^\dagger+\text{CD}$, the same as the experimental data. However, while using $\text{DJ16A}^* + \text{Coulomb}$, and USDCm interactions, the ordering of 0_2^+ and 2_2^+ was reversed for ^{18}Ne . On the other hand, all five interactions employed in this work are able to reproduce the correct ordering of states only up to the second excited state (4_1^+) for the neutron-rich partner. The ordering of 0_2^+ and 2_2^+ states were reversed compared to the experimental data.

Out of the six energy levels shown in Figure 8, 2_2^+ and 3_1^+ show large experimental MEDs of -304.04(74) and -816.8(102), respectively. In fact, the MED of 3_1^+ for this $A = 18$ pair is one of the highest among the *sd*-shell nuclei [14]. In Figure 10, a comparison between the calculated and experimentally observed MEDs is shown (fourth panel) along with the single orbital average occupancies of valence nucleons corresponding to $\text{DJ16A}^\dagger+\text{CD}$ (first panel), $\text{DJ16A}^\dagger+\text{w/SRC}$ (second panel) and USDCm (third panel). The calculated MED of 2_2^+ state using USDCm is in good agreement with the experimental MED value, while the same is around -440 keV for both $\text{DJ16A}^\dagger+\text{CD}$ and $\text{DJ16A}^\dagger+\text{w/SRC}$. On the other hand, the calculated MEDs of 3_1^+ state for $\text{DJ16A}^\dagger+\text{CD}$ and $\text{DJ16A}^\dagger+\text{w/SRC}$ are -586 and -615 keV, respectively, are better than USDCm result of -355 keV. Although the calculated MEDs for the $A = 18$ pair are far away from the experimental MED, such large theoretical MEDs can be explained by the large occupancies of $1s_{1/2}$. Surprisingly, the calculated MEDs of 0_2^+ state are quite large (around -700 keV) for both $\text{DJ16A}^\dagger+\text{CD}$ and $\text{DJ16A}^\dagger+\text{w/SRC}$ interactions, contrary to the experimental MED of -57.46(211) keV. The calculated MED of the same state with USDCm was -504 keV, whose strength is again higher than the experimental data. The highest average occupancies of valence $1s_{1/2}$ orbital among the six low-lying states are responsible for such enhancement in theoretical MED. On the other hand, the $\text{DJ16A}^* + \text{Coulomb}$ interactions significantly underpredict the experimental MEDs same as the $|T_z| = 1/2$ pair cases.

$^{22}\text{Mg}/^{22}\text{Ne}$: The calculated low-energy spectra of ($^{22}\text{Mg} - ^{22}\text{Ne}$) mirror pair is shown in Figure 9 along with the experimental data. It can be seen that the calculated spectra of $A = 22$ nuclei are in good agree-

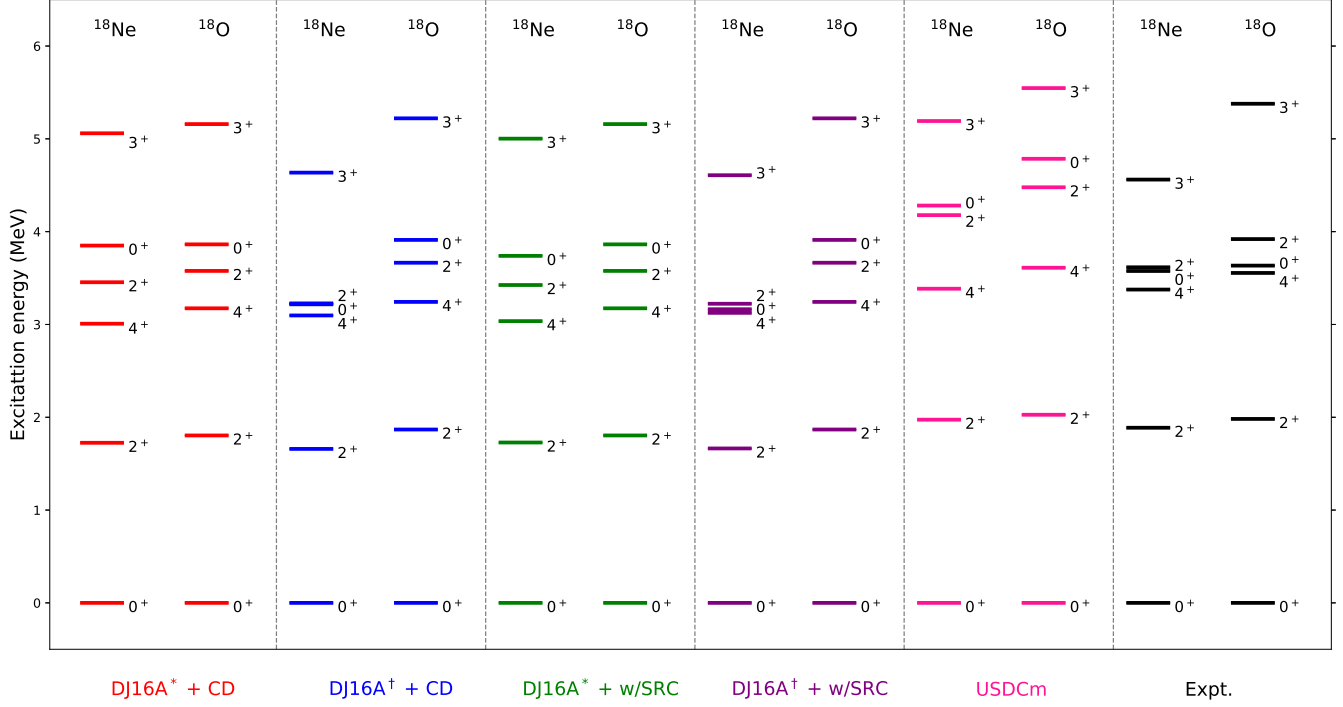


FIG. 8. Calculated low-energy spectra of $|T_z| = 1$ mirror pair ($^{18}\text{Ne} - ^{18}\text{O}$) using DJ16A*+CD, DJ16A†+CD, DJ16A*+w/SRC, DJ16A†+w/SRC and USDCm interactions are compared to the experimental data [70].

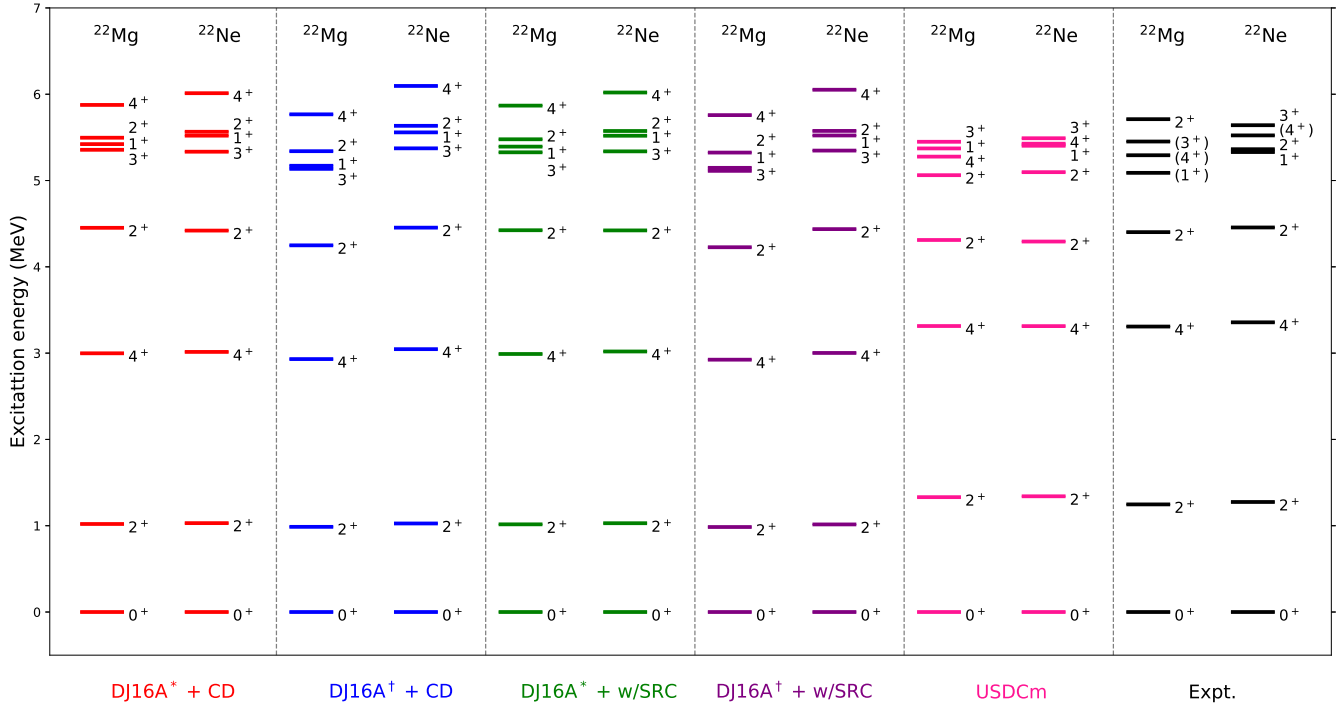


FIG. 9. Calculated low-energy spectra of $|T_z| = 1$ mirror pair ($^{22}\text{Mg} - ^{22}\text{Ne}$) using DJ16A*+CD, DJ16A†+CD, DJ16A*+w/SRC, DJ16A†+w/SRC and USDCm interactions are compared to the experimental data [70].

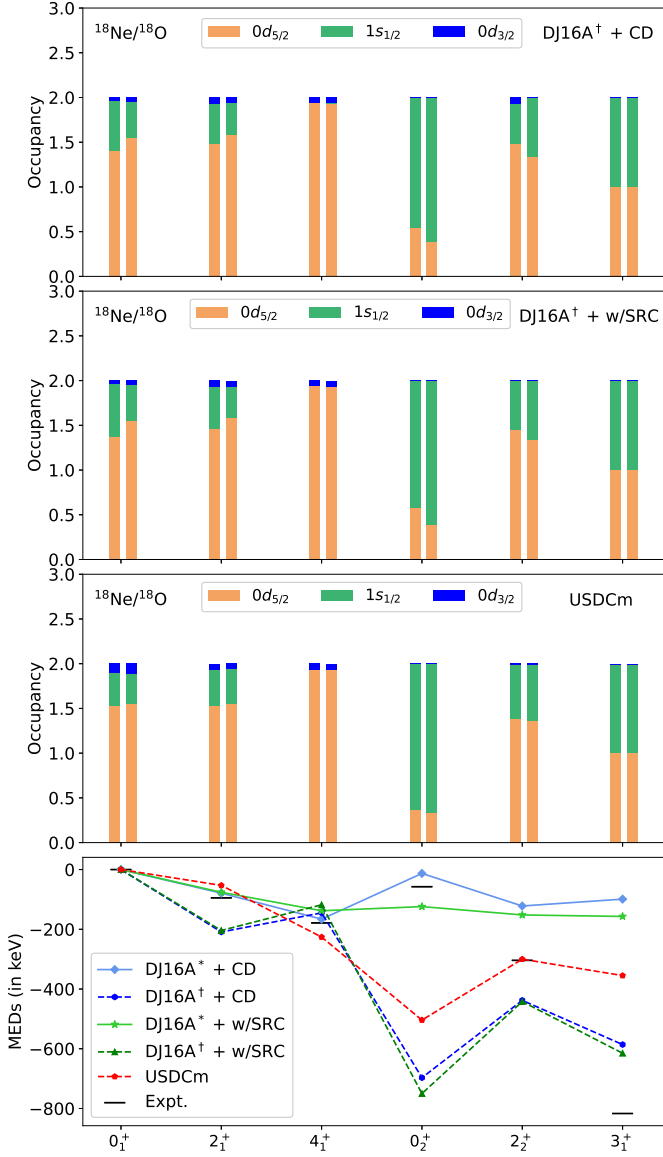


FIG. 10. Calculated average single orbital occupancies and MEDs for low-lying states of mirror pair ($^{18}\text{Ne} - ^{18}\text{O}$), using DJ16A[†]+CD, DJ16A[†]+w/SRC and USDCm interactions are shown. The displayed average occupancies correspond to the valence protons and neutrons in the respective mirror pair.

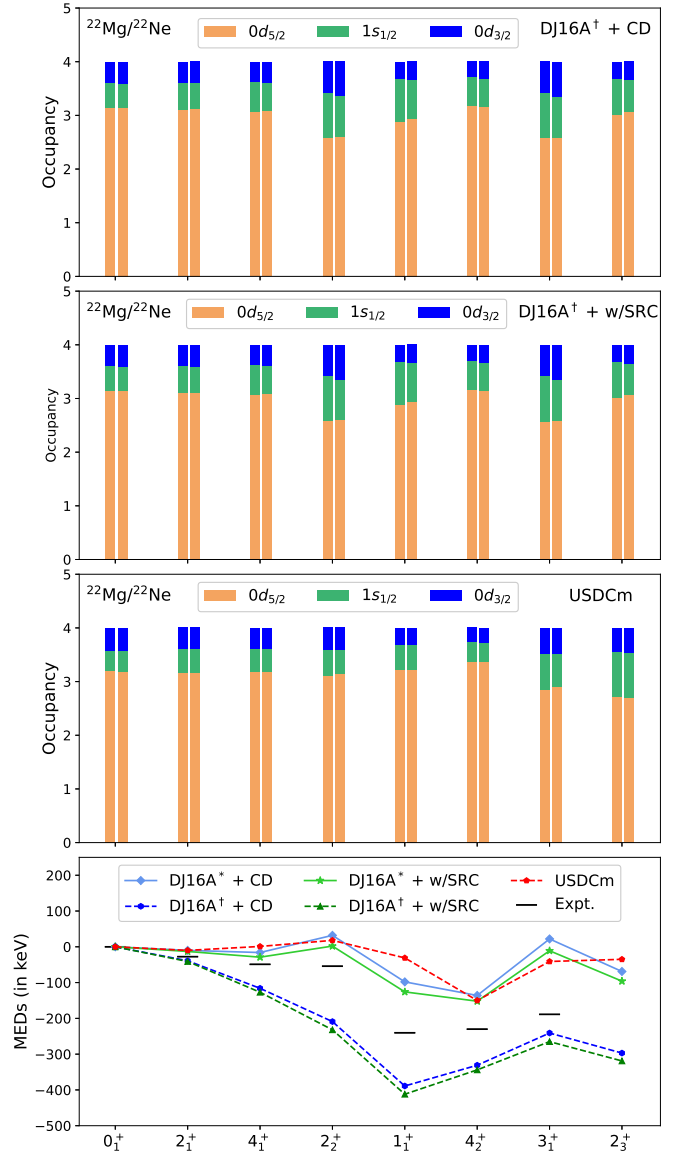


FIG. 11. Calculated average single orbital occupancies and MEDs for low-lying states of mirror pair ($^{22}\text{Mg} - ^{22}\text{Ne}$), using DJ16A[†]+CD, DJ16A[†]+w/SRC and USDCm interactions are shown. The displayed average occupancies correspond to the valence protons and neutrons in the respective mirror pair.

ment with the experimental data up to the third excited state (2_2^+). However, the excitation energies of 2_1^+ and 4_1^+ states obtained using both DJ16A-based interactions are almost 200 and 300 keV less than the experimental excitation energies, respectively, while the USDCm shows good agreement with the experimental data. The other four states are not in good agreement with any of the shell-model interactions. On the proton-rich side, 1_1^+ , 4_2^+ , and 3_1^+ states have transitional spin-parities, while only 4_2^+ state has un-confirmed spin-parity on the neutron-rich side.

In Figure 11, a comparison between the calculated and experimentally measured MEDs is shown (fourth panel), along with the single orbital average occupancies of valence nucleons corresponding to DJ16A † +CD, DJ16A † +w/SRC, and USDCm. Out of the eight low-lying states considered in this work, all four states above 2_2^+ show large MEDs. The experimentally measured MEDs of states 1_1^+ , 4_2^+ and 3_1^+ are -240.3(21), -230.19(76), and -188.8(11), respectively. The calculated MEDs in these three states corresponding to USDCm are -31, -150, and -41 keV, respectively, and underpredict the experimental data. On the other hand, the DJ16A † + Coulomb interactions show some more deviation from the experimental data. A significant disagreement between the calculated and experimental results is observed in the case of 2_3^+ . While the experimental MED of this state is 348.0(18) keV, the calculated MEDs for DJ16A † -based interactions are around -300 keV, while it is -35 keV for the USDCm interaction. DJ16A * + Coulomb interactions underpredict the experimental MEDs as was seen for other mirror pairs considered in this work.

C. Electromagnetic properties of mirror nuclei

The $E2$ transition strengths between different states of nuclei are in close relationship with the collectivity or deviations from a spherical shape. In this section, we discuss the $E2$ transition strengths of a few $|T_z| = 1/2$ and $|T_z| = 1$ mirror pairs across the sd -space. The calculated results corresponding to ISB sd -shell interactions DJ16A * +CD, DJ16A † +CD, DJ16A * +w/SRC, DJ16A † +w/SRC, and USDCm are compared to the experimental data. The effective charges of $e_p = 1.36e$ and $e_n = 0.45e$ are taken for all shell model calculations. The calculated $E2$ transition strengths for $|T_z| = 1/2$ nuclei from $A = 19$ to 31 are shown in Table III. The calculated $E2$ transition strengths for DJ16A-based interactions are consistent with the USDCm results except for ^{25}Al and ^{29}Si . While the $B(E2; 1/2^+ \rightarrow 5/2^+)$ of ^{25}Al and $B(E2; 3/2^+ \rightarrow 1/2^+)$ of ^{29}Si are underpredicted by the DJ16A-based interactions, the USDCm show overprediction for these two transitions. By comparing the results from columns fifth and seventh (or sixth and eighth) of Table III, it can be concluded that the difference in the Coulomb interactions has a small effect on the calculated $E2$ transition strengths. On the other hand, if we

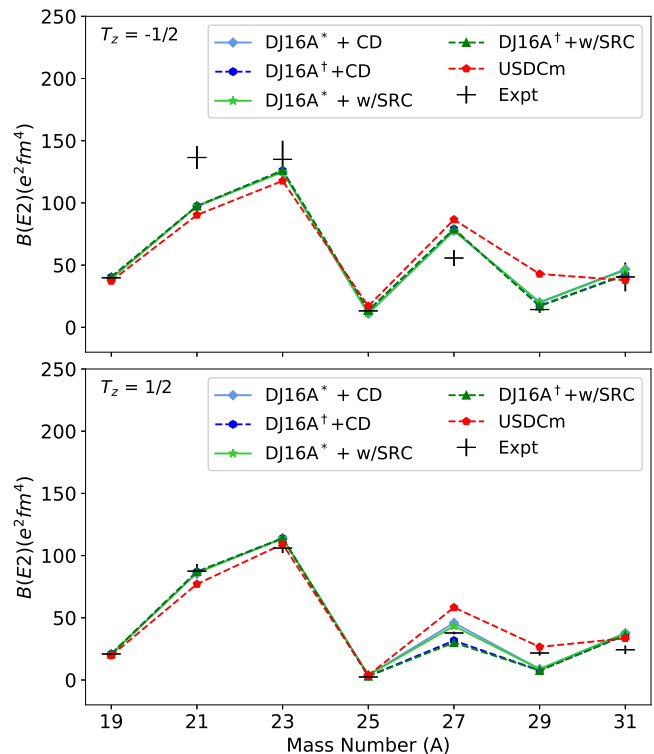


FIG. 12. The calculated $B(E2)$ values of $T_z = -1/2$ (top panel) and $T_z = 1/2$ (bottom panel) nuclei using DJ16A * +CD, DJ16A † +CD, DJ16A * +w/SRC, DJ16A † +w/SRC and USDCm interactions are compared to the experimental data.

compare the calculated $E2$ transition strengths from the fifth and sixth columns (or seventh and eighth columns) of Table III, the difference between the calculated results show that the effects of CSB + CIB interactions have sizable effects on the $B(E2)$. In Table IV, the $E2$ transition strengths of $|T_z| = 1$ mirror pairs from $A = 18$ to 30 are shown. The shell model results corresponding to the DJ16A-based interactions show that the $E2$ transition strengths are consistent with the USDCm results, except for ^{26}Si and $A = 30$ pair. By comparing the results of DJ16A-based interactions from the third to the sixth columns from Table IV, a similar conclusion can be drawn that CSB+CIB parts have sizable effects on the $E2$ transition strengths. A comparison between the experimental and calculated $E2$ transition strengths for $|T_z| = 1/2$ and $|T_z| = 1$ mirror pairs are also shown in Figure 12 and Figure 13, respectively.

We further investigated the isoscalar (M_0) and isovector (M_1) matrix elements for the $E2$ transition strengths reported in Table III and Table IV corresponding to three ISB interactions (DJ16A † + CD, DJ16A † + w/SRC, and USDCm) and compared them with the experimental data

TABLE III. The calculated $B(E2)$ values of $|T_z| = \frac{1}{2}$ sd -shell nuclei using different interactions, namely DJ16A*+CD, DJ16A[†]+CD, DJ16A*+w/SRC, DJ16A[†]+w/SRC, and USDCm are compared to the experimental data. The effective charges of $e_p = 1.36e$ and $e_n = 0.45e$ are taken for shell model calculations.

Isotope	J_i^π J_f^π		Expt.	B(E2) _↓ [e ² fm ⁴]				
				DJ16A*+CD	DJ16A [†] +CD	DJ16A*+w/SRC	DJ16A [†] +w/SRC	USDCm
¹⁹ Ne	$\frac{5}{2}_1^+$	$\frac{1}{2}_1^+$	39.8 (15) [70]	39.1	40.4	39.3	40.5	37.2
¹⁹ F	$\frac{5}{2}_1^+$	$\frac{1}{2}_1^+$	20.9 (2) [70]	20.6	20.9	20.7	21.0	19.6
²¹ Na	$\frac{5}{2}_1^+$	$\frac{3}{2}_1^+$	136.5 (92) [70]	97.4	97.4	97.4	97.4	90.3
²¹ Ne	$\frac{5}{2}_1^+$	$\frac{3}{2}_1^+$	87.5 (58) [70]	86.1	87.1	86.3	87.1	77.1
²³ Mg	$\frac{5}{2}_1^+$	$\frac{3}{2}_1^+$	135 (15) [28]	124.9	126.1	125.0	126.2	117.7
²³ Na	$\frac{5}{2}_1^+$	$\frac{3}{2}_1^+$	106 (4) [28]	113.9	113.9	113.9	113.9	109.2
²⁵ Al	$\frac{1}{2}_1^+$	$\frac{5}{2}_1^+$	13.2 (3) [70]	10.9	13.4	11.3	13.5	17.0
²⁵ Mg	$\frac{1}{2}_1^+$	$\frac{5}{2}_1^+$	2.44 (4) [70]	4.0	3.1	3.9	3.1	3.8
²⁷ Si	$\frac{1}{2}_1^+$	$\frac{5}{2}_1^+$	55.7 (64) [70]	77.6	79.3	77.8	79.2	86.6
²⁷ Al	$\frac{1}{2}_1^+$	$\frac{5}{2}_1^+$	37.8 (11) [70]	45.9	31.7	43.4	30.0	58.3
²⁹ P	$\frac{3}{2}_1^+$	$\frac{1}{2}_1^+$	14.3 (27) [70]	20.2	17.3	19.8	17.0	42.9
²⁹ Si	$\frac{3}{2}_1^+$	$\frac{1}{2}_1^+$	21.7 (21) [70]	8.8	7.7	8.7	7.6	26.6
³¹ S	$\frac{3}{2}_1^+$	$\frac{1}{2}_1^+$	40.5 (116) [70]	46.7	42.3	46.0	41.8	37.8
³¹ P	$\frac{3}{2}_1^+$	$\frac{1}{2}_1^+$	24.3 (35) [70]	37.7	36.3	37.4	36.1	33.5

TABLE IV. The calculated $B(E2)$ values of $|T_z| = 1$ sd -shell nuclei using different interactions, namely DJ16A*+CD, DJ16A[†]+CD, DJ16A*+w/SRC, DJ16A[†]+w/SRC, and USDCm are compared to the experimental data. The effective charges of $e_p = 1.36e$ and $e_n = 0.45e$ are taken for shell model calculations. All transitions are from the first excited state (2_1^+) to the g.s. (0_1^+).

Isotope	Expt.	B(E2) _↓ [e ² fm ⁴]				
		DJ16A*+CD	DJ16A [†] +CD	DJ16A*+w/SRC	DJ16A [†] +w/SRC	USDCm
¹⁸ Ne	49.6 (50) [70]	29.2	31.7	29.6	31.9	30.4
¹⁸ O	9.3 (3) [70]	3.3	3.3	3.3	3.3	3.3
²² Mg	76.2 (92) [71]	69.6	70.1	69.7	70.2	66.1
²² Ne	46.9 (5) [70, 71] [†]	54.7	55.6	54.8	55.7	49.9
²⁶ Si	70.0 (69) [70]	65.9	72.0	66.7	72.6	47.7
²⁶ Mg	61.3 (26) [70]	76.8	78.6	77.1	78.8	69.4
³⁰ S	68.7 (40) [70]	45.6	42.8	45.5	42.9	58.1
³⁰ Si	49.9 (65) [70]	30.1	37.0	30.8	37.9	47.1

[†] - Weighted average of values in Ref. [70] and Ref. [71]

following the formalism of Ref. [72]. The M_0 and M_1 matrix elements are defined as

$$M_0 = \frac{\sqrt{B(E2; T_z < 0)} + \sqrt{B(E2; T_z > 0)}}{2} \quad (7)$$

and

$$M_1 = \frac{\sqrt{B(E2; T_z < 0)} - \sqrt{B(E2; T_z > 0)}}{\Delta T_z} \quad (8)$$

The ratios of experimental to calculated isoscalar (M_0) and isovector (M_1) matrix elements are shown in Figure 14. The figures on the left show the ratios of M_0 for DJ16A[†]+CD (top-left panel), DJ16A[†]+w/SRC (middle-left panel), and USDCm (bottom-left panel). On the other hand, the figures on the right show the same

for M_1 using the same sets of interactions. The figure shows that the calculated isoscalar matrix elements exhibit small deviations from the experimental M_0 matrix elements compared to the isovector matrix elements. Also, among the M_0 matrix elements, the USDCm results show more spread compared to both DJ16A[†]+CD and DJ16A[†]+w/SRC results, particularly for $A = 25, 27,$ and 29 pairs. On the other hand, calculated M_1 matrix elements for $A = 18, 19,$ and 30 pairs were close to the experimental matrix elements; however other pairs showed significant deviations. In fact, the M_1 matrix element obtained for the USDCm interaction corresponding to $B(E2; 2_1^+ \rightarrow 0_1^+)$ transition of $A = 26$ pair reported in Table IV is almost three times larger than the experimental M_1 matrix element with a large error bar.

IV. SUMMARY AND CONCLUSIONS

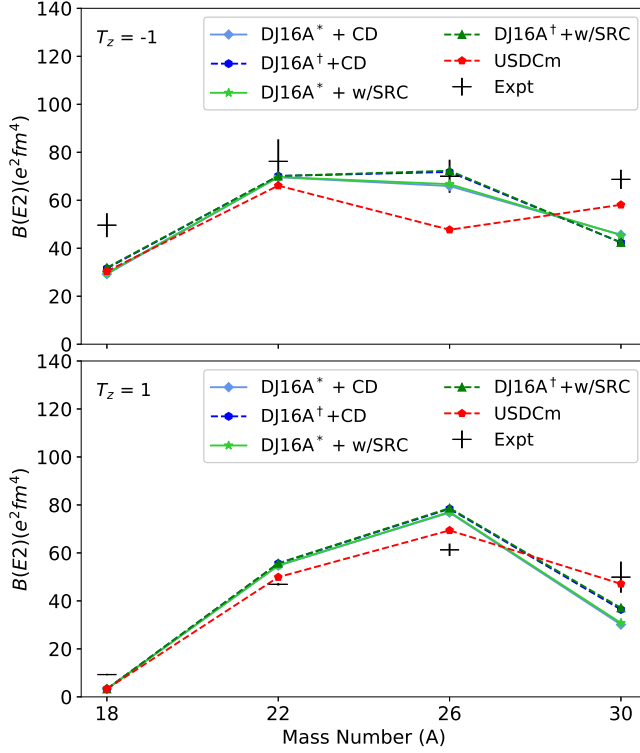


FIG. 13. The calculated $B(E2)$ values of $T_z = -1$ (top panel) and $T_z = 1$ (bottom panel) nuclei using DJ16A*+CD, DJ16A†+CD, DJ16A*+w/SRC, DJ16A†+w/SRC and USDCm interactions are compared to the experimental data.

Now, we focus on the ratios of M_0 and M_1 matrix elements corresponding to $|T_z| = 1/2$ pairs: $A = 25$ and 29 and $|T_z| = 1$ pair $A = 26$ for which at least one of the $E2$ transition strengths using DJ16A†+CD and DJ16A†+w/SRC interactions is far away from the USDCm results. From Figure 14, it can be seen that for the $A = 25$ pair, both M_0 and M_1 ratios for DJ16A†+CD and DJ16A†+w/SRC are small compared to the ratios for USDCm. On the other hand, while the M_0 matrix elements of $A = 26$ pair corresponding to DJ16A†+CD and DJ16A†+w/SRC are slightly higher than the USDCm matrix element, the M_1 matrix element for USDCm is much higher than the other two interactions. Finally, the calculated M_1 matrix elements of $A = 29$ pair are almost the same for all three interactions, and the difference in $E2$ transition strength between USDCm and DJ16A-based interactions are isoscalar in nature.

In this work, we have developed and tested the ISB versions of the DJ16A interaction. Starting from the isospin symmetric version of this interaction from Ref. [37], we added two different Coulomb interactions, Coulomb-CD and Coulomb-w/SRC, and we also added the phenomenological CSB and CIB effects to them. Additionally, we also considered the CSB and CIB part of the AV18 interaction. Finally, we considered four sets of interactions for each Coulomb interaction: (i) DJ16A + CD (w/SRC) combines isospin symmetric DJ16A interaction with a Coulomb part without considering the CSB and CIB effects, (ii) DJ16A + CSB^Y + CD (w/SRC) additionally combines the phenomenological CSB interaction to DJ16A + CD (w/SRC), (iii) DJ16A†+CD (w/SRC) takes into account Coulomb, CSB^Y and CIB^Y interactions and they are tuned to reproduce experimental $b(A = 17)$, $b(A = 18)$ and $c(A = 18)$, and (iv) DJ16A* + CD (w/SRC) is same as (iii) interactions with replacement of CSB^Y and CIB^Y by CSB^{AV18}} and CIB^{AV18}}, respectively, and without any reduction in the CIB strength. We then employed DJ16A*+CD (w/SRC) and DJ16A†+CD (w/SRC) interactions along with the USDCm to calculate the b -parameters of $|T_z| = 1/2$ and $|T_z| = 1$ nuclei across sd -shell and compared them with the experimental data. Based on the b_{rms} values of the g.s. of $|T_z| = 1/2$ and $|T_z| = 1$ nuclei across sd -shell, the DJ16A*+CD, and DJ16A†+CD interactions showed low b_{rms} up to $A = 33$ mirror pair. Additionally, we calculated the c -parameters for the $|T_z| = 1$ nuclei across sd -shell. The calculated c -parameters using all four DJ16A-based interactions along with the USDCm interaction are able to reproduce the staggering pattern of the experimental data correctly.

We then employed these interactions to calculate MEDs in the low-energy spectra of a few mirror nuclei pairs around $A = 20$ and compared them to the recently developed USDCm results and experimental data. For this work, $|T_z| = 1/2$ pairs: ($^{19}\text{Ne} - ^{19}\text{F}$) and ($^{21}\text{Na} - ^{21}\text{Ne}$) and $|T_z| = 1$ pairs: ($^{18}\text{Ne} - ^{18}\text{O}$) and ($^{22}\text{Mg} - ^{22}\text{Ne}$) were considered which have at least one low-energy state with large MED (larger than 200 keV). We also showed the relationship between such large MEDs and average occupancies of different valence orbitals. It is seen that large MEDs primarily occur due to large occupancies of $1s_{1/2}$, and minor contributions also come from the large occupancies of $0d_{3/2}$. The inclusion of phenomenological CSB and CIB effects in the DJ16A-based interactions leads to larger MEDs compared to the USDCm results in most cases. On the other hand, the inclusion of CSB and CIB effects from AV18 interaction shows underprediction compared to the experimental MEDs in most cases. Finally, we calculated the $E2$ transition strengths of a few $|T_z| = 1/2$ and $|T_z| = 1$ mirror pairs using all four DJ16A-based interactions along with the USDCm interaction and compared them with the experimental data. The shell model re-

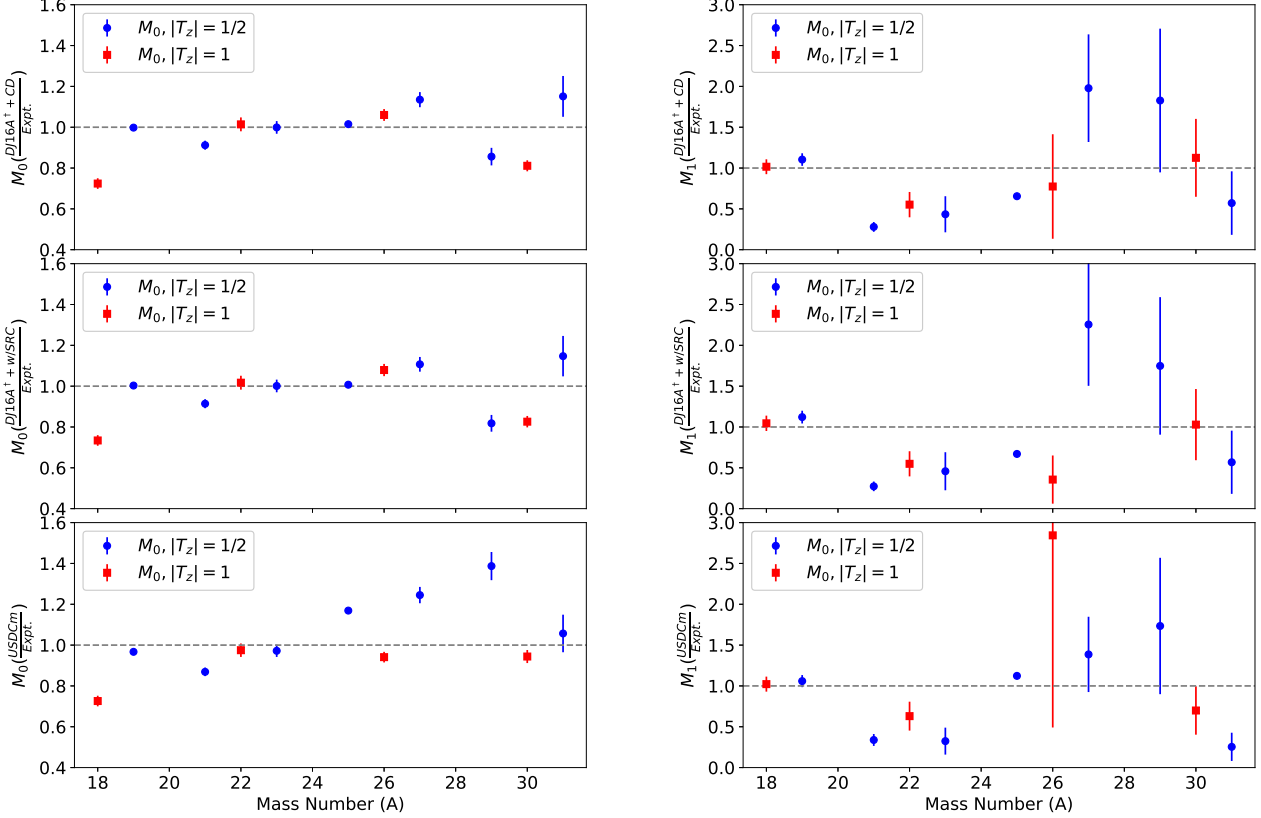


FIG. 14. (a) The ratios of experimental to calculated M_0 are shown for DJ16A † +CD (top panel), DJ16A † +w/SRC (middle panel), and USDCm (bottom panel); (b) ratios of experimental to calculated M_1 are shown for DJ16A † +CD (top panel), DJ16A † +w/SRC (middle panel), and USDCm (bottom panel)

sults are, on average, in good agreement with the experimental data. Almost the same $B(E2)$ values for both DJ16A † +CD and DJ16A † +w/SRC (DJ16A * +CD and DJ16A * +w/SRC) suggest that the effects of the difference in Coulomb interaction on $E2$ transitions are quite small. On the other, the difference in $B(E2)$ values for DJ16A * +CD and DJ16A † +CD (DJ16A * +w/SRC and DJ16A † +w/SRC) having same Coulomb part but different CSB+CIB part suggest a sizable effect on the calculated $E2$ transition strengths. Further, we calculated the ratios of theoretical to experimental isoscalar (M_0) and isovector (M_1) components for those transitions corresponding to DJ16A † +CD, DJ16A † +w/SRC, and USDCm interactions. While the M_0 ratios are close to the unity line for all three interactions, the M_1 ratios show significant deviations in some cases.

From the above discussions, it can be concluded that while DJ16A † +CD provides better results in terms of the b parameters up to $A = 33$ pairs, both of the DJ16A-based interactions with phenomenological CSB+CIB

part show overprediction of MEDs in a few cases around $A = 20$ mirror pairs. Contrary to this overprediction of MEDs, the DJ16A * +CD and DJ16A † +CD interactions with CSB+CIB from the AV18 interaction show underprediction of experimental MEDs in most cases. Among the four sets of interactions, the results of DJ16A † +CD results for b and c -parameters, MEDs, and $E2$ transition strengths are comparable to those of USDCm interaction. Therefore, DJ16A † +CD can serve as a complementary set of interactions to the newly developed USD-family interactions in Ref. [23]. These DJ16A-based microscopic ISB interactions can be tested for other mirror nuclei across sd -shell for nuclear structure properties and to study the ISB effects in the nuclear β -decay study.

ACKNOWLEDGMENTS

We acknowledge financial support from SERB (India), CRG/2022/005167, and MHRD India. The shell model calculations were performed using the KSHELL code [73].

- [1] W. Heisenberg, *Zeitschrift für Physik* **77**, 1-11 (1932).
- [2] E. Wigner, "On the consequences of the symmetry of the nuclear hamiltonian on the spectroscopy of nuclei", *Phys. Rev.* **51**, 106 (1937).
- [3] W. E. Ormand and B. A. Brown, "Calculated isospin-mixing corrections to Fermi β -decays in 1s0d-shell nuclei with emphasis on $A = 34$ ", *Nucl. Phys. A* **440**, 274 (1985).
- [4] W. E. Ormand and B. A. Brown, "Empirical isospin-nonconserving hamiltonians for shell-model calculations", *Nucl. Phys. A* **491**, 1 (1989).
- [5] N. A. Smirnova, "Isospin-symmetry breaking within the nuclear shell model: present status and developments", *Physics* **5**, 352-380 (2023).
- [6] P. Bączyk, J. Dobaczewski, M. Konieczka, W. Satuła, T. Nakatsukasa, and K. Sato, "Isospin-symmetry breaking in masses of $N = Z$ nuclei", *Phys. Lett. B* **778**, 178 (2018).
- [7] J. A. Sheikh, S. P. Rouoof, R. N. Ali, N. Rather, C. Sarma, and P. C. Srivastava, "Isospin symmetry breaking in atomic nuclei", *Symmetry* **16**, 745 (2024).
- [8] I.S.Towner, "Mirror asymmetry in allowed gamow-teller β -decay", *Nucl. Phys. A* **216**, 589 (1973).
- [9] N. A. Smirnova and C. Volpe, "On the asymmetry of Gamow-Teller β -decay rates in mirror nuclei in relation with second-class currents", *Nucl. Phys. A* **714**, 441 (2003).
- [10] B. Blank and M. J. G. Borge, "Nuclear structure at the proton drip line: Advances with nuclear decay studies", *Prog. Part. Nucl. Phys.* **60**, 403 (2008).
- [11] E. Hagberg, V. T. Koslowsky, J. C. Hardy, I. S. Towner, J. G. Hykawy, G. Savard, and T. Shinozuka, "Tests of Isospin Mixing Corrections in Superallowed $0^+ \rightarrow 0^+ \beta$ Decays", *Phys. Rev. Lett.* **73**, 396 (1994).
- [12] E. Farnea et al., "Isospin mixing in the $N=Z$ nucleus ^{64}Ge ", *Phys. Lett. B* **551**, 56 (2003).
- [13] A. P. Zuker, S. M. Lenzi, G. Martínez-Pinedo, and A. Poves, "Isobaric Multiplet Yrast Energies and Isospin Nonconserving Forces", *Phys. Rev. Lett.* **89**, 142502 (2002).
- [14] D.W.Bardayan et al., "Observation of the Astrophysically Important 3^+ State in ^{18}Ne via Elastic Scattering of a Radioactive ^{17}F Beam from ^1H ", *Phys. Rev. Lett.* **83**, 45 (1999).
- [15] R. G. Thomas, "An Analysis of the Energy Levels of the Mirror Nuclei, C^{13} and N^{13} ", *Phys. Rev.* **88**, 1109 (1952).
- [16] J. B. Ehrman, "On the Displacement of Corresponding Energy Levels of C^{13} and N^{13} ", *Phys. Rev.* **81**, 412 (1951).
- [17] M.A. Bentley, S.M. Lenzi, "Coulomb energy differences between high-spin states in isobaric multiplets", *Prog. Part. Nucl. Phys.* **59**, 497 (2007).
- [18] C. Yuan, C. Qi, F. Xu, T. Suzuki, and T. Otsuka, "Mirror energy difference and the structure of loosely bound proton-rich nuclei around $A = 20$ ", *Phys. Rev. C.* **89**, 044327 (2014).
- [19] Y. H. Lam, N. A. Smirnova, and E. Caurier, "Isospin non-conservation in sd -shell nuclei", *Phys. Rev. C* **87**, 054304 (2013).
- [20] B. H. Wildenthal, "Empirical strengths of spin operators in nuclei", *Prog. Part. Nucl. Phys.* **11**, 5 (1984).
- [21] B. A. Brown and B. H. Wildenthal, "Status of the Nuclear Shell Model", *Annu. Rev. Nucl. Part. Sci.* **38**, 29 (1988).
- [22] B. A. Brown and W. A. Richter, "New "USD" Hamiltonians for the sd shell", *Phys. Rev. C* **74**, 034315 (2006).
- [23] A. Magilligan and B. A. Brown, "New isospin-breaking "USD" Hamiltonians for the sd shell", *Phys. Rev. C* **101**, 064312 (2020).
- [24] S. Sahoo and P. C. Srivastava, "Isoscalar, isovector and orbital contributions in $M1$ transitions from analogous $M1$ and Gamow-Teller transitions in $T = 1/2$ mirror nuclei", *arXiv.2405.17119* (2024).
- [25] M. S. Martin, S. R. Stroberg, J. D. Holt, and K. G. Leach, "Testing isospin symmetry breaking in ab initio nuclear theory", *Phys. Rev. C.* **104**, 014324 (2022).
- [26] H. H. Li, J. G. Li, M. R. Xie, and W. Zuo, "Ab initio calculations of mirror energy difference in sd -shell nuclei", *Chinese Phys. C* **47**, 124101 (2023).
- [27] H. H. Li, Q. Yuan, J. G. Li, M. R. Xie, S. Zhang, Y. H. Zhang, X. X. Xu, N. Michel, F. R. Xu, and W. Zuo, "Investigation of isospin-symmetry breaking in mirror energy difference and nuclear mass with ab initio calculations", *Phys. Rev. C* **107**, 014302 (2023).
- [28] J. Henderson, G. Hackman, et al., "Coulomb excitation of the $|T_z| = 1/2$, $A = 23$ mirror pair", *Phys. Rev. C* **105**, 034332 (2022).
- [29] S. R. Stroberg, J. Henderson, G. Hackman, P. Ruotsalainen, G. Hagen, and J. D. Holt, "Systematics of $E2$ strength in the sd shell with the valence-space in-medium similarity renormalization group", *Phys. Rev. C* **105**, 034333 (2022).
- [30] T. Beck, A. Gade, B. A. Brown, et al., "Probing proton cross-shell excitations through the two-neutron removal from ^{38}Ca ", *Phys. Rev. C.* **108**, L061301 (2023).
- [31] S. A. Gillespie, K. W. Brown, R. J. Charity, et al., "Proton decay spectroscopy of ^{28}S and ^{30}Cl ", *Phys. Rev. C.* **105**, 044321 (2022).
- [32] S. E. Campbell, G. Bollen, B. A. Brown, et al., "Precision Mass Measurement of the Proton Dripline Halo Candidate ^{22}Al ", *Phys. Rev. Lett.* **132**, 152501 (2024).
- [33] J. G. Li, H. H. Li, S. Zhang, Y. M. Xing, and W. Zuo, "Double-magicity of proton drip-line nucleus ^{22}Si with ab initio calculation", *Phys. Lett. B* **846**, 138197 (2023).
- [34] C. Sarma, and P. C. Srivastava, "Nuclear structure study of $^{20-23}\text{Na}$ isotopes with ab initio no-core shell-model", *arXiv:2310.17893*.
- [35] A.F. Lisetskiy, B.R. Barrett, M.K.G. Kruse, P. Navrátil, I. Stetcu, J.P. Vary, "Ab-initio shell model with a core", *Phys. Rev. C* **78**, 044302 (2008).
- [36] E. Dikmen, A. F. Lisetskiy, B. R. Barrett, P. Maris, A.M. Shirokov, J.P. Vary, "Ab initio effective interactions for sd-shell valence nucleons", *Phys. Rev. C* **91**, 064301 (2015).
- [37] N. A. Smirnova, B. R. Barrett, Y. Kim, I. J. Shin, A. M. Shirokov, E. Dikmen, P. Maris, and J. P. Vary, "Effective interactions in the sd shell", *Phys. Rev. C* **100**, 054329 (2019).
- [38] T. T. S. Kuo and G. E. Brown, "Structure of finite nuclei and the free nucleon-nucleon interaction: An application to ^{18}O and ^{18}F ", *Nucl. Phys.* **85**, 40 (1966).
- [39] T. T. S. Kuo and G. E. Brown, "Reaction matrix elements for the 0f-1p shell nuclei", *Nucl. Phys.* **114**, 241 (1968).
- [40] S. Cohen and D. Kurath, "Effective interactions for the 1p shell", *Nucl. Phys.* **73**, 1 (1965).

- [41] A. Poves, J. Sanchez-Solano, E. Caurier, and F. Nowacki, "Shell model study of the isobaric chains $A = 50$, $A = 51$ and $A = 52$ ", *Nucl. Phys. A* **694**, 157 (2001).
- [42] M. Honma, T. Otsuka, B. A. Brown, and T. Mizusaki, "New effective interaction for pf -shell nuclei and its implications for the stability of the $N = Z = 28$ closed core", *Phys. Rev. C* **69**, 034335 (2004).
- [43] T. Otsuka, A. Gade, O. Sorlin, T. Suzuki, and Y. Utsuno, "Evolution of shell structure in exotic nuclei", *Rev. Mod. Phys.* **92**, 015002 (2020).
- [44] E. Caurier, G. M-Pinedo, F. Nowacki, A. Poves, and A. P. Zuker, "The shell model as a unified view of nuclear structure", *Rev. Mod. Phys.* **77**, 427 (2005).
- [45] B. R. Barrett, P. Navrátil, and J. P. Vary, "Ab initio no core shell model", *Prog. Part. Nucl. Phys.* **69**, 131 (2013).
- [46] H. Hergert, S. Binder, A. Calci, J. Langhammer, and R. Roth, "Ab Initio Calculations of Even Oxygen Isotopes with Chiral Two-Plus-Three-Nucleon Interactions", *Phys.Rev.Lett.* **110**, 242501 (2013).
- [47] S. K. Bogner, H. Hergert, J. D. Holt, A. Schwenk, S. Binder, A. Calci, J. Langhammer, and R. Roth, "Nonperturbative Shell-Model Interactions from the In-Medium Similarity Renormalization Group", *Phys. Rev. Lett.* **113**, 142501 (2014).
- [48] G. R. Jansen, J. Engel, G. Hagen, P. Navratil, and A. Signoracci, "Ab Initio Coupled-Cluster Effective Interactions for the Shell Model: Application to Neutron-Rich Oxygen and Carbon Isotopes", *Phys. Rev. Lett.* **113**, 142502 (2014).
- [49] P. Choudhary, P. C. Srivastava, and P. Navrátil, "Ab initio no-core shell model study of $^{10-14}\text{B}$ isotopes with realistic NN interactions", *Phys. Rev. C* **102**, 044309 (2020).
- [50] P. Choudhary, P. C. Srivastava, M. Gennari, and P. Navrátil, "Ab initio no-core shell-model description of $^{10-14}\text{C}$ isotopes", *Phys. Rev. C* **117**, 014309 (2023).
- [51] A. Saxena and P. C. Srivastava, "Ab initio no-core shell model study of $^{18-23}\text{O}$ and $^{18-24}\text{F}$ isotopes", *J. Phys. G: Nucl. Part. Phys.* **47**, 055113 (2020).
- [52] C. Sarma and P. C. Srivastava, "Ab-initio no-core shell model study of $^{18-24}\text{Ne}$ isotopes", *J. Phys. G: Nucl. Part. Phys.* **50**, 045105 (2023).
- [53] A. Shirokov, A. Mazur, J. Vary, and T. Weber, "Realistic nuclear Hamiltonian: Ab exitu approach", *Phys. Lett. B* **644**, 33 (2007).
- [54] D. R. Entem and R. Machleidt, "Accurate charge-dependent nucleon-nucleon potential at fourth order of chiral perturbation theory", *Phys. Rev. C* **68**, 041001(R) (2003).
- [55] A. M. Shirokov, I. J. Shin, Y. Kim, M. Sosonkina, P. Maris, and J. P. Vary, "N3LO NN interaction adjusted to light nuclei in ab exitu approach" *Phys. Lett. B* **761**, 87 (2016).
- [56] K. Suzuki and R. Okamoto, "Effective interaction theory and unitary-model-operator approach to nuclear saturation problem", *Prog. Theor. Phys.* **92**, 1045 (1994).
- [57] P. Choudhary and P.C. Srivastava, "Study of S, Cl and Ar isotopes with $N \geq Z$ using microscopic effective sd-shell interactions", *Eur. Phys. J. A* **59**, 97 (2023).
- [58] P. Choudhary and P. C. Srivastava, "Nuclear structure properties of Si and P isotopes with the microscopic effective interactions", *Nucl Phys. A* **1033**, 122629 (2023).
- [59] S. Sahoo, P. C. Srivastava, and T. Suzuki, "Study of structure and radii for $^{20-31}\text{Na}$ isotopes using microscopic interactions", *Nucl. Phys. A* **1032**, 122618 (2023).
- [60] C. Sarma, O. D. Matteo, A. Abhishek, and P. C. Srivastava, "Prediction of the neutron drip line in oxygen isotopes using quantum computation", *Phys. Rev. C* **108**, 064305 (2023).
- [61] Z. Li, N. A. Smirnova, A. M. Shirokov, I. J. Shin, B. R. Barrett, P. Maris, J. P. Vary, "Effective operators for valence space calculations from the ab initio No-Core Shell Model", [arXiv:2205.15939](https://arxiv.org/abs/2205.15939).
- [62] G. A. Miller and J. E. Spencer, "A survey of pion charge-exchange reactions with nuclei", *Ann. Phys. (NY)* **100**, 562 (1976).
- [63] J. A. Nolen, J.P. Schiffer, "Coulomb Energies", *Ann. Rev. Nucl. Sci.* **1969**, 19, 471–526.
- [64] T. Suzuki, H. Sagawa, and N. V. Giai, "Charge independence and charge symmetry breaking interactions and the Coulomb energy anomaly in isobaric analog states", *Phys. Rev. C* **47**, R1360(R) (1993).
- [65] T. Suzuki, H. Sagawa, and A. Arima, "Effects of valence nucleon orbits and charge symmetry breaking interaction on the Nolen-Schiffer anomaly of mirror nuclei", *Nucl. Phys. A* **536**, 141 (1992).
- [66] R. B. Wiringa, V. G. J. Stoks, and R. Schiavilla, "Accurate nucleon-nucleon potential with charge-independence breaking", *Phys. Rev. C* **51**, 38 (1995).
- [67] E. P. Wigner, in Proceedings of the Robert A. Welch Foundation Conference on Chemical Research, edited by W. O. Milligan, Vol. 1 (Welch Foundation, Houston, 1957), p. 86.
- [68] M. Wang, W. J. Huang, F. G. Kondev, G. Audi, and S. Naimi, "The AME 2020 atomic mass evaluation (II). Tables, graphs and references", *Chinese Phys. C* **45**, 030003 (2020).
- [69] M. R. Hall, D. W. Bardayan, T. Baugher, *et al.*, " ^{19}Ne level structure for explosive nucleosynthesis". *Phys. Rev. C* **102**, 045802 (2020).
- [70] Evaluated Nuclear Structure Data File (ENSDF), <http://www.nndc.bnl.gov/ensdf/>.
- [71] J. Henderson, G. Hackman, P. Ruotsalainen, S. R. Stroberg, K.D. Launey, J.D. Holt, *et al.*, "Testing microscopically derived descriptions of nuclear collectivity: Coulomb excitation of ^{22}Mg ", *Phys. Lett. B* **782**, 468 (2018).
- [72] B. A. Brown, B. H. Wildenthal, W. Chung, S. E. Massen, M. Bernas, A. M. Bernstein, R. Miskimen, V. R. Brown, and V. A. Madsen, "Isovector $E2$ matrix elements from electromagnetic transitions in the s - d shell: Experiment and shell-model calculations", *Phys. Rev. C* **26**, 2247 (1982).
- [73] N. Shimizu, T. Mizusaki, Y. Utsuno and Y. Tsunoda, "Thick-restart block Lanczos method for large-scale shell-model calculations", *Comput. Phys. Comm.* **244**, 372 (2019).